The Energy Correlation Coefficient and its Key Role in Wirelessly Powered Networks

Na Deng, *Member, IEEE*, and Martin Haenggi, *Fellow, IEEE*

***Abstract*—Energy correlation critically affects the performance of a wirelessly powered network due to its key effect on the spatial distribution of concurrent RF-powered transmitters. This paper introduces a powerful analytical framework with foundations in stochastic geometry to characterize the energy correlation in a general wirelessly powered network. Unlike the commonly used pair correlation function (pcf)-based method, it is based on the *energy correlation coefficient* (ECC) and yields the energy correlation distance that gives a sufficiently small ECC. Specifically, we focus on the spatial correlation of the energy harvested from a Poisson field of RF power sources with directional beams under two cases: i) each power source points the beam in a random direction; ii) each power source points the beam to an RF-powered node located in its Voronoi cell. The results demonstrate that the energized RF-powered nodes in both cases exhibit positive correlation that is weaker than in the omni-directional case due to the introduction of energy beamforming. As an application, we provide an ECC-based method using the energy correlation distance to approximate the success probability and area spectral efficiency in the communication phase. It turns out that the ECC-based approximation matches the exact result well, and, more importantly, it can deal with the energy correlation in more general and complicated scenarios (where the pcf analysis is infeasible) due to its superior tractability.**

***Index Terms*—Energy correlation; wirelessly powered networks; directional energy transfer; stochastic geometry.**

I. Introduction

A. Motivation

Radio frequency (RF) energy harvesting is a promising solution to realize self-sustainable communications, especially for energy-constrained networks such as sensor networks and the Internet of Things [2–4]. The integration of RF energy harvesting and communications brings new challenges and opportunities and calls for a paradigm shift in wireless network design. Many efforts have recently been made towards addressing these new research problems that cover a wide range of disciplines. Among them, advancing the theoretical understanding of wirelessly powered communication systems is an essential direction of research. Accordingly, stochastic geometry has naturally been a popular tool for the modeling and analysis of large-scale wirelessly powered networks [5].

Na Deng is with the School of Information and Communication Engineering, Dalian University of Technology, Dalian, 116024, China (e-mail: dengna@dlut.edu.cn). Martin Haenggi is with the Dept. of Electrical Engineering, University of Notre Dame, Notre Dame 46556, USA (e-mail: mhaenggi@nd.edu).

Part of this work is presented at the 2021 IEEE International Conference on Communications (ICC'21) [1].

This work was supported by the National Natural Science Foundation of China under Grant 61701071, by the Fundamental Research Funds for the Central Universities (DUT21JC04), and by the US National Science Foundation under Grant 2007498.

Regardless of the kind of wireless network being powered, the main idea behind the majority of existing works is to model the locations of RF power sources as a homogeneous Poisson point process (PPP) and investigate the first-order performance metric, i.e., the average energy transfer success probability (or, equivalently, the energization probability of RF-powered nodes). Then, the energized RF-powered nodes, i.e., the active transmitters in the communication phase, are simply assumed to form another homogeneous PPP independent of the RF power sources [5–9]. While this leads to tractable results, the analytical insights provided are quite limited since the spatial correlation of the energy harvested from RF transmitters is not taken into account. Our previous work [10] named this correlation *energy correlation*, which is shown to exist and be positive. As a result, the locations of the active RF-powered nodes in the communication phase are not mutually independent but clustered. This reveals that the energy correlation needs to be fully characterized in order to get the accurate spatial configuration of the active transmitters in the communication phase, which plays a critical role in the performance evaluation of wirelessly powered networks.

The study of energy correlation requires the joint analysis of the harvested energies observed at two different locations, which is known to be significantly more challenging than the popular approach that confines the analysis to a single location, i.e., the first-order performance described above. The pair correlation function (pcf) is by far the most commonly used measure to characterize the second-order statistics of the point process in stochastic geometry [11]. Although the energy correlation has already been characterized for wirelessly powered networks through the pcf, the resulting expression is too complicated to evaluate and thus replaced by an approximation in [10, 12]. More importantly, the previous study on energy correlation is limited to the omni-directional energy harvesting scenario, and the situation is quite different for the directional energy harvesting scenario where the pcf analysis is far more challenging. But in practice, RF signals suffer from high attenuation over longer distances, which implies that directional energy harvesting techniques need to be implemented to improve the energy transfer efficiency [13]. Therefore, currently, a thorny issue is that a simple but efficient evaluation of the energy correlation and its effect on the performance of a more general (including directional energy transfer) wirelessly powered network is elusive.

B. Related Work

Energy harvesting techniques utilizing RF signals have lately gained a lot of attention in both academia and in-

dustry, as they provide an appealing tetherless approach to supply power to energy-constrained devices. This has led to considerable research which can be broadly divided into two categories: wirelessly powered communication networks (WPCNs)[1] [2] and simultaneous wireless information and power transfer (SWIPT)-enabled networks [14]. In either case, the harvested energy is positively correlated with the aggregate signal strength, which, in turn, strongly depends on the spatial configuration of RF power sources. As a consequence, stochastic geometry tools have been widely used to analyze the performance of wireless energy transfer (WET) and WET-enabled networks (see, e.g., [5–10, 12, 15, 16] and references therein).

A main application of stochastic geometry in RF energy harvesting-based wireless communication is to model the locations of RF power sources using the homogeneous PPP model, which permits the derivation of metrics like average harvested energy, energy coverage/outage probability, joint distribution of harvested power and rate, etc. To be specific, the authors in [5] studied an uplink cellular network overlaid with power beacons (PBs) powering mobiles, where PBs form a homogeneous PPP independent of the locations of the mobiles. Under an outage constraint, tradeoffs between the transmission power of PBs and mobiles as well as the densities of PBs and base stations were analyzed. The authors in [15] leveraged stochastic geometry for modeling SWIPT-enabled cellular networks and characterized the tradeoff between wireless information and power transmission through the joint cumulative distribution function of harvested power and rate, where the locations of RF power sources were also modeled by a PPP. As extensions, several authors further investigated the performance of various wirelessly powered communication (WPC) and SWIPT-enabled types of wireless networks, e.g., device-to-device networks [6, 8], ad hoc networks [7], cognitive networks [9], heterogeneous cellular networks [16, 17] and IoT networks [18]. Although these papers provide answers to different important design issues, they have one limitation in common: the spatial correlation of the energized RF-powered nodes is not considered. For SWIPT, such correlation is not critical since the RF transmitters serve as the transmitters in both energy and information transfer phases, while for WPCN, only the RF-powered nodes that harvest enough energy become active in the communication phase. Accordingly, the spatial configuration of these energized RF-powered nodes plays an important role in analyzing the communication performance. Motivated by this insight, we explored the correlation of the harvested energy in a WPCN and proposed a new point process, named *energized point process* (EPP), as a model for the RF-powered nodes that succeed in harvesting enough energy [10]. However, since the spatial distribution of the points in the EPP highly depends on the energy transfer phase, i.e., the energy and information transfer phases are closely related, an exact characterization of the WET-enabled communication performance is infeasible. Considering the accuracy and tractability tradeoff, we then promoted the Poisson disk process (PDP), an intermediate class between the PPP and the EPP, for modeling the energized RF-powered nodes and analyzed the information transmission success probability in WPCNs [12].

The energy correlation is induced in the energy transfer phase and affects the spatial configuration of transmitters in the communication phase—it essentially establishes a bridge between the performance of the energy and information transfer phases. While there have been many studies on the performance analysis for RF energy harvesting-based wireless networks, research on the aforementioned energy correlation is still in its infancy. The existing approach in capturing the energy correlation is to first specify a point process of the energized RF-powered nodes, e.g., the EPP, and then investigate the spatial correlation of the point process through the pcf. However, explicit expressions for the pcf are not always available; for instance, when energy beamforming techniques are considered, the beam direction will cause extra correlation between two RF-powered nodes relative to the omni-directional case studied in existing works [10, 12]. As a result, the joint analysis of the energy harvesting success probabilities at two locations becomes quite challenging and hence the pcf-based method in this case seems infeasible. To avoid this problem, this paper introduces the *energy correlation coefficient* (ECC), namely the correlation coefficient of the measured energy at two locations, to capture the correlation structure directly from the energy field induced by the power sources. Different from the traditional pcf-based method, it is applicable even if the spatial distribution of the energized RF-powered nodes is not known. Hence, the ECC-based method can deal with the energy correlation in more general and complicated scenarios (e.g., directed energy transfer), thereby unlocking a new avenue to gain design insights on WPCNs with energy beamforming.

C. Contributions

In this paper, we provide a new analytical approach to investigate the energy correlation and its effects on the communication performance. It is not based on a complicated pcf analysis and subsequent point process fitting, which makes it suitable for a wider range of WPCN scenarios. The main contributions are:

- We provide the exact ECC under the random directed energy transfer (RDET) policy and a simple yet effective approximation of the ECC under the nearest directed energy transfer (NDET) policy in WPCNs, where the energy is harvested from a Poisson field of RF power sources.
- We analyze the asymptotic behaviors of the energy correlation under RDET and NDET policies with respect to the antenna array size.
- We show that, remarkably, for directed WET, the energy correlation is positive but weaker than in the omni-directional case, and when the antenna array size tends to infinity, the correlation in the RDET policy vanishes while the one in the NDET policy approaches a positive constant.

[1]In WPCNs, wireless devices use harvested RF energy to transmit/decode information to/from other devices [2]. It is envisioned to apply to many popular commercial and industrial systems in the future, including but not limited to IoT/IoE systems as well as large-scale wireless sensor networks.

- We provide analytical expressions for the density of energized RF-powered nodes under the two energy beamforming policies.
- We introduce the *energy correlation distance*, which is the distance where the ECC is sufficiently small for the energies harvested to be considered uncorrelated, and based on it, we propose the ECC-based method as a highly accurate approximation to the WET-enabled communication performance.

II. System model

A. Network model

We consider a wireless network powered solely by ambient RF power sources (such as dedicated power beacons, cellular base stations, WiFi hotspots, digital TV towers, etc.) with locations modeled by a homogeneous PPP $\Phi_{\rm p} \subset \mathbb{R}^2$ of density $\lambda_{\rm p}$. We assume that each RF power source is equipped with a uniform linear array (ULA) composed of $N_{\rm p}$ antenna elements to perform directional energy beamforming, and each RF-powered node has a single antenna. The channel (power) gain between transmitter x and receiver y is given by $G_{xy}h_{xy}\ell(x-y)$, where G_{xy} is the antenna array gain determined by the energy beamforming policy, h_{xy} models the small-scale fading and $\ell(x-y)$ represents the large-scale path loss. We assume that the fading coefficient follows a gamma distribution $\mathrm{Gamma}(M, \frac{1}{M})$ (i.e., Nakagami fading), and all h_{xy} are mutually independent and also independent of the point process. We consider a bounded path loss law

$$\ell(x) = \frac{1}{\epsilon + \|x\|^{\alpha}}, \tag{1}$$

where $\epsilon > 0$ avoids a singularity at $\|x\| = 0$ and α is the path loss exponent. To maintain analytical tractability, a sectorized antenna model [19] is adopted to approximate the actual antenna pattern, and the antenna gain function is formulated as

$$G(\varphi) = \begin{cases} G_{\rm m} & \text{if } |\varphi| \le \frac{w}{2} \\ G_{\rm s} & \text{otherwise,} \end{cases} \tag{2}$$

where $\varphi \in [-\pi, \pi)$ is the angle off the beam direction of the RF power source, $w \in (0, 2\pi]$ is the half-power beam width (HPBW), correlated with the antenna array size, $G_{\rm m}$ and $G_{\rm s}$ are the array gains of the main and side lobes. Assuming a ULA with half-wavelength antenna spacing, we have $G_{\rm m} = N_{\rm p}$ and $w = 4\pi G_{\rm act}^{-1}(G_{\rm m}/2)$ with $G_{\rm act}(\varphi) = \frac{\sin^2(\pi N_{\rm p}\varphi)}{N_{\rm p}\sin^2(\pi\varphi)}$ denoting the actual antenna pattern [20]. To ensure the power constraint $\frac{1}{2\pi}\int_0^{2\pi} G(\varphi)\mathrm{d}\varphi = 1$, we have $G_{\rm s} = \frac{2\pi - G_{\rm m}w}{2\pi - w}$.

B. Wireless Energy Harvesting Model

The correlation coefficient of the measured energy at two locations is used to characterize the energy correlation caused by the specific energy beamforming policy. Due to the motion-invariance of the PPP, the correlation coefficient merely depends on the distance of two locations. Hence, without loss of generality, we focus on the measured energy at the origin o and $z = (d, 0)$.

Letting $\mathcal{E}(y)$ be the measured energy present at location y, the ECC is given by

$$\chi(d) = \frac{\mathbb{E}[\mathcal{E}(o)\mathcal{E}(z)] - \mathbb{E}\mathcal{E}(o)\mathbb{E}\mathcal{E}(z)}{\sqrt{\mathrm{var}(\mathcal{E}(o))\mathrm{var}(\mathcal{E}(z))}}, \tag{3}$$

and we consider two practical energy beamforming policies as follows.

1) Randomly directed energy transfer (RDET) policy: Each RF power source randomly selects the beam direction of the energy transfer link. Hence, for an RF-powered device located at y, its angle $\varphi_x(y)$ off the beam direction of each RF power source x is randomly and uniformly distributed in $[-\pi, \pi)$, and the antenna gain $G(\varphi_x(y))$ has the probability mass function (PMF)

$$G(\varphi_x(y)) = \begin{cases} G_{\rm m} & \text{w.p. } q_{\rm m} = \frac{w}{2\pi} \\ G_{\rm s} & \text{w.p. } q_{\rm s} = 1 - \frac{w}{2\pi}. \end{cases} \tag{4}$$

Using the linear energy harvesting model, the measured energy[2] $\mathcal{E}_{\rm R}(y)$ at y from all the RF power sources is quantified as

$$\mathcal{E}_{\rm R}(y) = \sum_{x\in\Phi_{\rm p}} G(\varphi_x(y))h_{xy}\ell(x-y). \tag{5}$$

2) Nearest directed energy transfer (NDET) policy: Each RF-powered device is associated with its nearest RF power source which aligns the beam direction pointing to one RF-powered device in its Voronoi cell[3]. If two or more RF-powered devices have the same nearest RF power source, the beam is pointed to the different devices in a time-division manner. If an RF power source has no devices in its Voronoi cell, it keeps silent. Letting $x_1 \in \Phi_{\rm p}$ be the nearest RF power source to the origin, pointing its beam to o, the measured energy at o is

$$\mathcal{E}_{\rm N}(o) = G_{\rm m}h_{x_1o}\ell(x_1) + \sum_{x\in\Phi_{\rm p}\setminus\{x_1\}} G(\varphi_x(o))h_{xo}\ell(x). \tag{6}$$

For the measured energy at z, we need to consider whether it has the same nearest RF power source x_1. Denote by $x_2 \in \Phi_{\rm p}$ the nearest RF power source to z. If $x_2 = x_1$, o and z are both in the Voronoi cell of x_1. In the ECC analysis, since the time instant considered is when the origin is getting the beam targeted toward it, the measured energy at z is

$$\begin{aligned}\mathcal{E}_{\rm N}(z) = {} & G(\varphi_{x_1}(z))h_{x_1z}\ell(x_1-z) \\ & + \sum_{x\in\Phi_{\rm p}\setminus\{x_1\}} G(\varphi_x(z))h_{xz}\ell(x-z),\end{aligned} \tag{7}$$

where $G(\varphi_{x_1}(z))$ depends on the angle $\varphi_{x_1}(z)$ off the beam direction of the RF power source x_1 (namely the direction from x_1 to o). If $x_2 \neq x_1$, o and z are located in different Voronoi cells, and we focus on a time instant where the beam

[2]The measured energy is the actual energy present at a location rather than the harvested energy which depends on the capabilities of RF-powered nodes, i.e., linear or non-linear energy harvesting. Since we focus on the linear model, the results are identical whether we consider measured or harvested energy.

[3]If the RF power sources are cellular base stations, the results of the NDET would apply to the case when the RF-powered device lies in the same direction as a served user.

TABLE I. Symbols and descriptions

Symbol	Description	Default value
$\Phi_{\rm p}$, $\lambda_{\rm p}$	RF power sources PPP and density	$\rm N/A, 0.1$
$\Phi_{\rm d}$, $\lambda_{\rm d}$	RF-powered nodes PPP and density	$\rm N/A, 1$
$\Phi_{\rm e}$, $\lambda_{\rm e}$	Energized RF-powered nodes EPP and density	$\rm N/A, N/A$
α, ϵ	The parameters of path loss law for the energy link	4, 0.01
M	The Nakagami parameter of the energy link	$\rm N/A$
$N_{\rm p}$	The antenna array size of RF power sources	8
$G_{\rm m}, G_{\rm s}, w$	The antenna gain of main and side lobes, and the HPBW	N/A
$\mathcal{E}_{\rm R}, \mathcal{E}_{\rm N}$	The harvested energy under RDET/NDET policy	N/A
d	The inter-point distance of two locations for ECC	0.1
$\chi_{\rm R}, \chi_{\rm N}$	The ECC under RDET/NDET policy	N/A
$\alpha_{\rm I}$	The path loss exponent for the information link	4
$E_{\rm th}, \theta$	The energy/SIR threshold	$\rm N/A, N/A$
$d_{\rm I}$	The distance between the transmitter-receiver pair for the information link	1
$D, \bar{c}$	The parameters of the Matérn cluster process	$\rm N/A, N/A$

from x_2 is pointed at z. Accordingly, the measured energy at z is

$$\mathcal{E}_{\rm N}(z) = G_{\rm m} h_{x_2 z} \ell(x_2 - z) + \sum_{x \in \Phi_{\rm p} \setminus \{x_2\}} G(\varphi_x(z)) h_{xz} \ell(x - z). \quad (8)$$

C. Communication Model

We further consider the information transmission performance in this WPCN where RF-powered devices are distributed as another homogeneous PPP $\Phi_{\rm d}$ of density $\lambda_{\rm d}$ and powered by the RF-power sources using the aforementioned two directional energy transfer policies. Each RF-powered device is assumed to have a dedicated receiver at distance $d_{\rm I}$ in a random orientation[4], with a fixed transmit power of one. Since only the active RF-powered nodes, i.e., the devices that succeed in harvesting enough energy, can actually participate in the communication phase, we need to focus on the EPP $\Phi_{\rm e}$, defined as a dependent thinning of $\Phi_{\rm d}$ as

$$\Phi_{\rm e} \triangleq \{x \in \Phi_{\rm d} \colon \mathcal{E}(x) > E_{\rm th}\}, \quad (9)$$

where $E_{\rm th}$ is the energy threshold. We assume that the path loss model in the information transmission phase is $\ell_{\rm I}(x) = \|x\|^{-\alpha_{\rm I}}$, and all power fading coefficients are i.i.d. exponential with mean one (Rayleigh fading).

For the information transmission phase, the received SIR is a strong performance indicator of a wireless link, and its distribution (or, equivalently, the information transmission success probability) depends upon the joint distribution of the received power from the desired transmitter and interferers. Since the EPP is a stationary point process, we condition on that the typical transmitter (active RF-powered node) is located at the origin, with the corresponding typical receiver at $z_{\rm I} = (d_{\rm I}, 0)$. Letting $\Phi_{\rm e}^o \triangleq (\Phi_{\rm e} \mid o \in \Phi_{\rm e})$ and $\Phi_{\rm e}^{!o} \triangleq \Phi_{\rm e}^o \setminus \{o\}$, the received SIR of the typical receiver is given by

$$\mathrm{SIR} = \frac{h_{oz_{\rm I}} \ell_{\rm I}(z_{\rm I})}{\sum\limits_{x \in \Phi_{\rm e}^{!o}} h_{xz_{\rm I}} \ell_{\rm I}(x - z_{\rm I})}. \quad (10)$$

[4]This is a standard model that allows an easy comparison with results available for conventionally-powered bipolar networks. If the distances are randomly distributed, the results require just an extra expectation that would mask the crisper insight we can get from making the distance deterministic. Also, the results are more general in the sense that they do not rely on a specific assumption on the distribution of the distances.

Table I summarizes the system parameters with their descriptions and default values.

III. Analysis of Energy Correlation Coefficient

In this section, we provide analytical results for the ECC at two locations and investigate the features of the energy correlation under RDET and NDET policies, respectively.

A. Analysis of RDET

In this policy, $\varepsilon_{\rm R}(o)$ and $\varepsilon_{\rm R}(z)$ are identically distributed but not independent, and we have

$$\chi_{\rm R}(d) = \frac{\mathbb{E}[\mathcal{E}_{\rm R}(o)\mathcal{E}_{\rm R}(z)] - \mathbb{E}[\mathcal{E}_{\rm R}(o)]^2}{\mathbb{E}[\mathcal{E}_{\rm R}(o)^2] - \mathbb{E}[\mathcal{E}_{\rm R}(o)]^2}. \quad (11)$$

Although each RF power source randomly selects the beam direction, the antenna array gains from an RF power source to two different locations are still correlated with each other, which affects the calculation of $\mathbb{E}[\mathcal{E}_{\rm R}(o)\mathcal{E}_{\rm R}(z)]$. As a result, we first give the PMF of $\widetilde{G}(x,z) = G(\varphi_x(o))G(\varphi_x(z))$ for an RF power source x in the following lemma.

Lemma 1. *Given that an RF power source is located at $x = (r\cos\theta, r\sin\theta)$, the PMF of $\widetilde{G}(x,z)$ is given by*

$$\widetilde{G}(x,z) = \begin{cases} G_{\rm m}^2 & \text{w.p. } \frac{w - \min(w,\nu)}{2\pi} \\ G_{\rm m} G_{\rm s} & \text{w.p. } \frac{\min(w,\nu)}{\pi} \\ G_{\rm s}^2 & \text{w.p. } 1 - \frac{w + \min(w,\nu)}{2\pi}. \end{cases} \quad (12)$$

where $\nu = \arccos\left(\frac{r - d\cos\theta}{\sqrt{r^2 + d^2 - 2rd\cos\theta}}\right)$ denotes the angle between the direction from x to o and z.

Proof: See Appendix A.

With the help of Lemma 1, we give the ECC in the RDET case in the following theorem.

Theorem 1. *Letting $\delta = 2/\alpha$ and $\zeta(x,z) = \mathbb{E}(\widetilde{G}(x,z) \mid x \in \Phi_{\rm p})$, the ECC of $\mathcal{E}_{\rm R}(o)$ and $\mathcal{E}_{\rm R}(z)$ with the RDET policy is given by*

$$\chi_{\rm R}(d) = \frac{M \sin(\pi\delta)}{M+1} \frac{\int_{\mathbb{R}^2} \zeta(x,z)\ell(x)\ell(x-z)\mathrm{d}x}{(G_{\rm m}^2 q_{\rm m} + G_{\rm s}^2 q_{\rm s})\pi^2 \delta(1-\delta)\epsilon^{\delta-2}}. \quad (13)$$

Proof: Firstly, using Campbell's theorem and $\mathbb{E}h_{xo}=1$, we have

$$\mathbb{E}\mathcal{E}_{\mathrm{R}}(o)=\lambda_{\mathrm{p}}\int_{\mathbb{R}^2}\mathbb{E}[G(\varphi_x(o))]\ell(x)\mathrm{d}x\overset{(a)}{=}\lambda_{\mathrm{p}}\int_{\mathbb{R}^2}\ell(x)\mathrm{d}x, \quad (14)$$

where step (a) uses the power constraint $G_{\mathrm{m}}q_{\mathrm{m}}+G_{\mathrm{s}}q_{\mathrm{s}}=1$. Secondly, the second moment of the harvested energy is given by

$$\begin{aligned}
&\mathbb{E}[\mathcal{E}_{\mathrm{R}}(o)^2]\\
&=\mathbb{E}\Big[\Big(\sum_{x\in\Phi_{\mathrm{p}}}G(\varphi_x(o))h_{xo}\ell(x)\Big)^2\Big]\\
&=\mathbb{E}\sum_{x\in\Phi_{\mathrm{p}}}G^2(\varphi_x(o))h_{xo}^2\ell^2(x)\\
&+\mathbb{E}\sum_{x,y\in\Phi_{\mathrm{p}}}^{x\neq y}G(\varphi_x(o))G(\varphi_y(o))h_{xo}h_{yo}\ell(x)\ell(y)\\
&\overset{(b)}{=}\lambda_{\mathrm{p}}\frac{M+1}{M}\int_{\mathbb{R}^2}\mathbb{E}[G^2(\varphi_x(o))]\ell^2(x)\mathrm{d}x\\
&+\lambda_{\mathrm{p}}^2\int_{\mathbb{R}^2}\int_{\mathbb{R}^2}\mathbb{E}[G(\varphi_x(o))]\ell(x)\mathbb{E}[G(\varphi_y(o))]\ell(y)\mathrm{d}x\mathrm{d}y\\
&=\lambda_{\mathrm{p}}\frac{(G_{\mathrm{m}}^2q_{\mathrm{m}}+G_{\mathrm{s}}^2q_{\mathrm{s}})(M+1)}{M}\int_{\mathbb{R}^2}\ell^2(x)\mathrm{d}x+\mathbb{E}[\mathcal{E}_{\mathrm{R}}(o)]^2\\
&\overset{(c)}{=}\lambda_{\mathrm{p}}\frac{(G_{\mathrm{m}}^2q_{\mathrm{m}}+G_{\mathrm{s}}^2q_{\mathrm{s}})(M+1)}{M}\frac{\pi^2\delta(1-\delta)\epsilon^{\delta-2}}{\sin(\pi\delta)}+\mathbb{E}[\mathcal{E}_{\mathrm{R}}(o)]^2,
\end{aligned} \quad (15)$$

where step (b) follows from the independence of h_{xo} and h_{yo}, $\mathbb{E}[h_{xy}^2]=\frac{M+1}{M}$, the independence of $G(\varphi_x(o))$ and $G(\varphi_y(o))$ as well as the second-order product density of the PPP [11], and step (c) follows from [21, Eq. 3.251.11]. Lastly, the mean of $\mathcal{E}_{\mathrm{R}}(o)\mathcal{E}_{\mathrm{R}}(z)$ is expressed as

$$\begin{aligned}
&\mathbb{E}[\mathcal{E}_{\mathrm{R}}(o)\mathcal{E}_{\mathrm{R}}(z)]\\
&=\mathbb{E}\Big[\sum_{x\in\Phi_{\mathrm{p}}}G(\varphi_x(o))h_{xo}\ell(x)\sum_{y\in\Phi_{\mathrm{p}}}G(\varphi_y(z))h_{yz}\ell(y-z)\Big]\\
&=\mathbb{E}\sum_{x\in\Phi_{\mathrm{p}}}G(\varphi_x(o))G(\varphi_x(z))h_{xo}\ell(x)h_{xz}\ell(x-z)\\
&+\mathbb{E}\sum_{x,y\in\Phi_{\mathrm{p}}}^{x\neq y}G(\varphi_x(o))G(\varphi_y(z))h_{xo}h_{yz}\ell(x)\ell(y-z)\\
&\overset{(d)}{=}\lambda_{\mathrm{p}}\int_{\mathbb{R}^2}\mathbb{E}[\widetilde{G}(x,z)]\ell(x)\ell(x-z)\mathrm{d}x\\
&+\lambda_{\mathrm{p}}^2\int_{\mathbb{R}^2}\int_{\mathbb{R}^2}\mathbb{E}[G(\varphi_x(o))]\ell(x)\mathbb{E}[G(\varphi_y(z))]\ell(y-z)\mathrm{d}x\mathrm{d}y\\
&=\lambda_{\mathrm{p}}\int_{\mathbb{R}^2}\zeta(x,z)\ell(x)\ell(x-z)\mathrm{d}x+\mathbb{E}[\mathcal{E}_{\mathrm{R}}(o)]^2,
\end{aligned} \quad (16)$$

where step (d) follows by similar reasoning as step (b). ∎

Remark 1. *This theorem shows that the ECC is positive and increases with the fading parameter M. Put differently, the small-scale fading reduces the energy correlation under the RDET policy. Since the interference in wireless networks is the aggregated signal power from all interfering transmitters (excluding the desired transmitter) and the measured energy is the aggregated one from all transmitters, the two correlations are closely related. In essence, they could be regarded as two instances of the same underlying problem of the correlation structure of a random field induced by Poisson-located emitters.*

When $N_{\mathrm{p}}=1$, the RDET policy reduces to the omni-directional energy transfer case, where the ECC corresponds to the interference correlation coefficient in [22, 23]. Since the interference correlation with directional beamforming has not been analyzed, the results of the ECC also solve that problem with the same path loss and fading models, i.e., the energy correlation equals the interference correlation.

Next, we find the ECC for the unbounded path-loss model by letting $\epsilon\to 0$.

Corollary 1. *Letting $\epsilon\to 0$, we have $\chi_{\mathrm{R}}(d)\to 0$ for $d\neq 0$.*

Proof: We have

$$\begin{aligned}
&\chi_{\mathrm{R}}(d)\\
&=\frac{M\sin(\pi\delta)}{M+1}\frac{\int_{\mathbb{R}^2}\frac{\zeta(x,z)}{(\epsilon+\|x\|^\alpha)(\epsilon+\|x-z\|^\alpha)}\mathrm{d}x}{(G_{\mathrm{m}}^2q_{\mathrm{m}}+G_{\mathrm{s}}^2q_{\mathrm{s}})\pi^2\delta(1-\delta)\epsilon^{\delta-2}}\\
&\overset{(a)}{=}\frac{M\sin(\pi\delta)}{M+1}\frac{\epsilon^{\delta-2}\int_{\mathbb{R}^2}\frac{\zeta(\epsilon^\delta x,z)}{(1+\|x\|^\alpha)(1+\|(x-\epsilon^{-\delta}z)\|^\alpha)}\mathrm{d}x}{(G_{\mathrm{m}}^2q_{\mathrm{m}}+G_{\mathrm{s}}^2q_{\mathrm{s}})\pi^2\delta(1-\delta)\epsilon^{\delta-2}},
\end{aligned} \quad (17)$$

where (a) follows from the change of variables. When $\epsilon\to 0$, we have $\chi_{\mathrm{R}}(d)\to 0$. ∎

This corollary shows that the unbounded path loss model yields zero ECC due to the dominant contribution of the nearby RF power sources to the measured energy. To be specific, for two locations o and z with distance $d\neq 0$, the measured energy at o and z is dominated by the RF power sources in disk $b(o,r)$ and $b(z,r)$, respectively, for a small r, which are independent for a PPP and thus make the ECC go to zero.

We further explore how the antenna array size N_{p} (or, equivalently, the beamwidth) affects the correlation and what happens when $N_{\mathrm{p}}\to\infty$.

Corollary 2. *Letting $N_{\mathrm{p}}\to\infty$, we have $\chi_{\mathrm{R}}(d)\to 0$.*

Proof: When $N_{\mathrm{p}}\to\infty$, we have $G_{\mathrm{m}}\to\infty$ and $w\to 0$. Furthermore, according to the power constraint, we have $G_{\mathrm{s}}<1$. Thus, it is obtained that

$$\widetilde{G}(x,z)=\begin{cases}G_{\mathrm{m}}G_{\mathrm{s}} & \text{w.p. } \frac{w}{\pi}\\ G_{\mathrm{s}}^2 & \text{w.p. } 1-\frac{w}{\pi},\end{cases} \quad (18)$$

and $\zeta(x,z)=\frac{w}{\pi}G_{\mathrm{m}}G_{\mathrm{s}}+(1-\frac{w}{\pi})G_{\mathrm{s}}^2$. Then, the ECC can be further expressed as

$$\begin{aligned}
\chi_{\mathrm{R}}(d)&=\frac{G_{\mathrm{m}}G_{\mathrm{s}}\frac{w}{\pi}+G_{\mathrm{s}}^2(1-\frac{w}{\pi})}{G_{\mathrm{m}}^2\frac{w}{2\pi}+G_{\mathrm{s}}^2(1-\frac{w}{2\pi})}\underbrace{\frac{M\int_{\mathbb{R}^2}\ell(x)\ell(x-z)\mathrm{d}x}{(M+1)\int_{\mathbb{R}^2}\ell^2(x)\mathrm{d}x}}_{\mathcal{A}}\\
&=\mathcal{A}\frac{2wG_{\mathrm{s}}+G_{\mathrm{s}}^2(\pi-w)/G_{\mathrm{m}}}{G_{\mathrm{m}}w+G_{\mathrm{s}}(2\pi-w)+(\frac{G_{\mathrm{s}}^2}{G_{\mathrm{m}}}-G_{\mathrm{s}})(2\pi-w)}\\
&=\mathcal{A}\frac{2wG_{\mathrm{s}}+G_{\mathrm{s}}^2(\pi-w)/G_{\mathrm{m}}}{2\pi+(\frac{G_{\mathrm{s}}^2}{G_{\mathrm{m}}}-G_{\mathrm{s}})(2\pi-w)}\to 0.
\end{aligned} \quad (19)$$

∎

Remark 2. *This corollary shows that the energy correlation at two locations vanishes when $N_{\rm p} \to \infty$, which implies that modeling the energized RF-powered devices by independent thinning is only accurate in the extreme case when the RF power sources are equipped with infinite antenna arrays.*

B. Analysis of NDET

In this policy, each RF power source points the beam to the RF-powered devices lying in its Voronoi region. As a consequence, the energy correlation between two RF-powered nodes under NDET is highly affected by whether the two RF-powered nodes have the same nearest RF power source, which significantly complicates the analysis. Since energy beamforming is employed and the NDET policy is designed to supply concentrated, stable and abundant energy directly to certain nodes, it is expected to make the nearest RF power source be the dominant energy supply source. Accordingly, for the sake of simplicity, the total harvested energy from all RF power sources is approximated by the harvested energy from the nearest RF power source, resulting in $\mathcal{E}_{\rm N}(o) \approx G_{\rm m} h_{x_1 o} \ell(x_1)$ and

$$\mathcal{E}_{\rm N}(z) \approx \begin{cases} G(\varphi_{x_1}(z)) h_{x_1 z} \ell(x_1 - z) & \text{if } x_2 = x_1 \\ G_{\rm m} h_{x_2 z} \ell(x_2 - z) & \text{if } x_2 \neq x_1. \end{cases} \tag{20}$$

To characterize the energy correlation, it is necessary to derive the distance distribution of $R_2 = \|x_2 - z\|$, which is given in the following lemma. For notational convenience, we define $R \triangleq \sqrt{r^2 + d^2 - 2rd\cos\theta}$, and

$$A(r_1, r_2, d) \triangleq \begin{cases} \pi(\min\{r_1, r_2\})^2, & d \leq |r_1 - r_2| \\ r_1^2\varphi_1 + r_2^2\varphi_2 - s_\Delta, & |r_1 - r_2| < d < r_1 + r_2 \\ 0, & \text{otherwise} \end{cases} \tag{21}$$

is the intersection area of two disks with radii r_1 and r_2 at distance d, where

$$\varphi_1 = \arccos\left(\frac{r_1^2 + d^2 - r_2^2}{2r_1 d}\right), \tag{22}$$

$$\varphi_2 = \arccos\left(\frac{r_2^2 + d^2 - r_1^2}{2r_2 d}\right), \tag{23}$$

$$s_\Delta = \frac{1}{2}\sqrt{[(r_1 + r_2)^2 - d^2][d^2 - (r_1 - r_2)^2]}. \tag{24}$$

When $r_1 = R$ and $r_2 = r$, we have a simple form of $A(r_1, r_2, d)$ for $\theta \in [0, \pi]$, given by

$$A(R, r, d) = R^2 \arccos\left(\frac{d - r\cos\theta}{R}\right) - r^2\theta + rd\sin\theta. \tag{25}$$

Lemma 2. *Given that the nearest RF power source to the origin x_1 is located at $(r\cos\theta, r\sin\theta)$, the two locations z and o have the same nearest RF power source with probability*

$$\varpi(r, \theta) = e^{-\lambda_{\rm p}(\pi R^2 - A(R, r, d))}, \tag{26}$$

and the unconditional probability is

$$p_{\rm same} = \int_0^\pi \int_0^\infty 2\lambda_{\rm p} r e^{-\lambda_{\rm p}\pi r^2} \varpi(r, \theta) {\rm d}r{\rm d}\theta. \tag{27}$$

Conditioned on $x_2 \neq x_1$, the cumulative distribution function of the distance R_2 is given by

$$F_{R_2}(r_2) = \begin{cases} \frac{1 - e^{-\lambda_{\rm p}(\pi r_2^2 - A(r_2, r, d))}}{1 - \varpi(r, \theta)} & r_2 \in [\psi(r), R] \\ 0 & \textit{otherwise}, \end{cases} \tag{28}$$

where $\psi(r) = \max(0, r - d)$.

Proof: See Appendix B.

With the help of Lemma 2, we next provide the approximate ECC under the NDET policy.

Theorem 2. *The ECC of $\mathcal{E}_{\rm N}(o)$ and $\mathcal{E}_{\rm N}(z)$ with the NDET policy is approximated as*

$$\chi_{\rm N}(d) \approx \frac{\xi_{zo} - \eta_o \eta_z}{\sqrt{(\kappa_o - \eta_o^2)(\kappa_z - \eta_z^2)}}, \tag{29}$$

where

$$\eta_o = \pi\lambda_{\rm p} \int_0^\infty \frac{e^{-\pi\lambda_{\rm p} r}}{\epsilon + r^{\alpha/2}} {\rm d}r, \tag{30}$$

$$\kappa_o = \pi\lambda_{\rm p} \frac{M + 1}{M} \int_0^\infty \frac{e^{-\pi\lambda_{\rm p} r}}{(\epsilon + r^{\alpha/2})^2} {\rm d}r, \tag{31}$$

$$\eta_z = \int_0^\pi \int_0^\infty 2\lambda_{\rm p} r e^{-\pi\lambda_{\rm p} r^2} \left[\frac{\varpi(r, \theta) G(r, \theta)}{\epsilon + R^\alpha} + \int_{\psi(r)}^R (1 - \varpi(r, \theta)) \frac{{\rm d}F_{R_2}(r_2)}{\epsilon + r_2^\alpha}\right] {\rm d}r{\rm d}\theta, \tag{32}$$

$$\kappa_z = \frac{M + 1}{M} \int_0^\pi \int_0^\infty 2\lambda_{\rm p} r e^{-\pi\lambda_{\rm p} r^2} \left[\frac{\varpi(r, \theta) G^2(r, \theta)}{(\epsilon + R^\alpha)^2} + \int_{\psi(r)}^R (1 - \varpi(r, \theta)) \frac{{\rm d}F_{R_2}(r_2)}{(\epsilon + r_2^\alpha)^2}\right] {\rm d}r{\rm d}\theta, \tag{33}$$

$$\xi_{zo} = \int_0^\pi \int_0^\infty 2\lambda_{\rm p} r e^{-\pi\lambda_{\rm p} r^2} \left[\frac{\varpi(r, \theta) G(r, \theta)}{(\epsilon + r^\alpha)(\epsilon + R^\alpha)} + \int_{\psi(r)}^R (1 - \varpi(r, \theta)) \frac{{\rm d}F_{R_2}(r_2)}{(\epsilon + r^\alpha)(\epsilon + r_2^\alpha)}\right] {\rm d}r{\rm d}\theta, \tag{34}$$

and

$$G(r, \theta) = \begin{cases} 1 & \textit{if } |\arccos(\frac{r - z\cos(\theta)}{R})| \leq \frac{w}{2} \\ G_{\rm s}/G_{\rm m} & \textit{otherwise}. \end{cases} \tag{35}$$

Proof: See Appendix C.

It is observed that increasing M reduces both κ_o and κ_z and thus increases the ECC under the NDET policy. When $N_{\rm p} = 1$, the NDET policy also reduces to the omni-directional energy transfer case, and the ECC has exactly the same expression as in the RDET policy under the assumption that all RF power sources are active. Next, we investigate what happens to the energy correlation in the NDET case when $N_{\rm p} \to \infty$.

Corollary 3. *Letting $N_{\rm p} \to \infty$, we have*

$$\chi_{\rm N}(d) \to \frac{\tilde{\xi}_{zo} - \eta_o \tilde{\eta}_z}{\sqrt{(\kappa_o - \eta_o^2)(\tilde{\kappa}_z - \tilde{\eta}_z^2)}}, \tag{36}$$

where

$$\tilde{\eta}_z = \int_0^\pi \int_0^\infty \int_{\psi(r)}^R 2\lambda_{\rm p} r e^{-\pi\lambda_{\rm p} r^2} \frac{(1 - \varpi(r, \theta)) {\rm d}F_{R_2}(r_2)}{\epsilon + r_2^\alpha} {\rm d}r{\rm d}\theta,$$

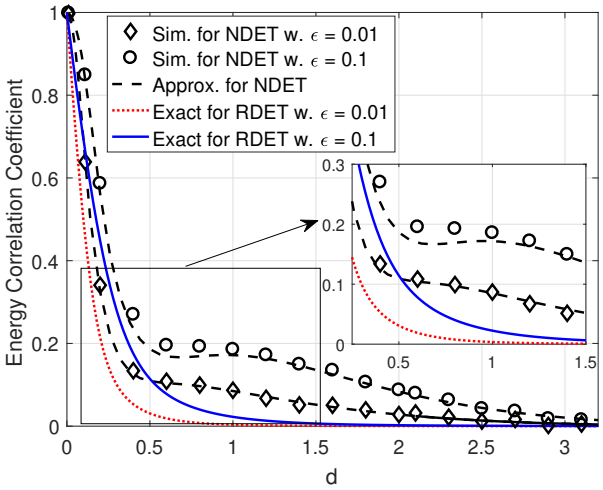

Fig. 1. The ECCs versus the inter-point distance for the RDET and NDET with different ϵ.

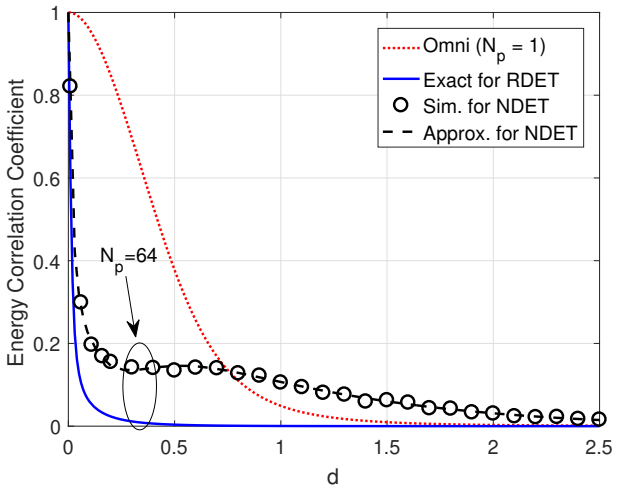

Fig. 2. The comparison of ECCs between the omni-directional and directional energy transfer policies.

$$\tilde{\kappa}_z = \frac{2\lambda_{\rm p}(M+1)}{M}\int_0^{\pi}\int_0^{\infty}\int_{\psi(r)}^{R}\frac{re^{-\pi\lambda_{\rm p}r^2}(1-\varpi(r,\theta))\mathrm{d}F_{R_2}(r_2)}{(\epsilon+r_2^{\alpha})^2}\mathrm{d}r\mathrm{d}\theta,$$

$$\tilde{\xi}_{zo} = \int_0^{\pi}\int_0^{\infty}\int_{\psi(r)}^{R} 2\lambda_{\rm p}re^{-\pi\lambda_{\rm p}r^2}\frac{(1-\varpi(r,\theta))\mathrm{d}F_{R_2}(r_2)}{(\epsilon+r^{\alpha})(\epsilon+r_2^{\alpha})}\mathrm{d}r\mathrm{d}\theta.$$

Proof: When $N_{\rm p}\to\infty$, we have $w\to 0$ and $\frac{G_{\rm s}}{G_{\rm m}}\to 0$. ■

Remark 3. *This corollary implies that the correlation of the measured energy at two locations does not disappear when $N_{\rm p}\to\infty$, which means that the EPP under NDET cannot be simply approximated by independently thinning the point process of RF-powered devices.*

Fig. 1 plots the ECC as a function of the distance d with different ϵ for RDET and NDET. To verify the approximation results in the NDET policy, we provide simulation results corresponding to the case where all RF power sources are considered rather than merely the nearest one. It can be seen that the approximate analytical results of the NDET policy match the simulation results well, which confirms the accuracy and effectiveness of the proposed approximation. From the overall trend, the ECCs for both policies are positive and mostly decrease with the increase of d, finally tending to zero for all parameter settings. The difference is that NDET yields a larger ECC that decreases to zero at a lower rate than RDET. This is because the random directed policy reduces the energy correlation. Moreover, it is observed that a smaller ϵ leads to a weaker energy correlation. The reason is that the nearby RF power sources usually contribute more energy to RF-powered nodes than the others, and as ϵ decreases, their contributions become more dominant to the total measured energy when $\alpha=4$.

Fig. 2 compares the ECCs between the omni-directional ($N_{\rm p}=1$) and directional ($N_{\rm p}=64$) energy transfer policies as a function of d. It is observed that the ECC in the omni-directional case is always higher than in the RDET case. The reason is that the omni-directional policy provides the same antenna gain to the two different locations while the RDET policy provides the antenna gains in a more random way. When compared with the NDET, the omni-directional policy yields a larger ECC for $d<0.75$ but a smaller ECC for $d>0.75$. For a smaller d in the NDET policy, the two RF-powered nodes are more likely to be located in the same Voronoi cell but have different antenna gains, which leads to the ECC curve lying in between the omni and RDET cases. Comparatively, for a larger d, the two RF-powered nodes are likely to be located in different Voronoi cells, and each of them is powered by an energy transfer beam directing to it. In this case, the energy correlation comes from the geometric correlation between the nearest RF power sources of the two RF-powered nodes. When d is moderate, say around $d=0.6$, the ECC depends on the probability of each of the above cases occurring. However, due to the difference in the energy beamforming policy, the geometric correlation does not yield a comparable energy correlation in the omni-directional policy as in the NDET policy.

Fig. 3 illustrates the ECC versus the antenna array size $N_{\rm p}$ for different d under the RDET and NDET policies. For the RDET policy, it is shown that the ECC decreases with the increase of $N_{\rm p}$. This is because the amount of the measured energy highly depends on the main lobe of the RF power source, and a narrower beam formed by a larger antenna array decreases the probability that two RF-powered nodes are covered by the main lobe of the same RF power source. In other words, narrowing the beamwidth decreases the energy correlation. Compared with the RDET, NDET is more complicated and its ECC curves are more interesting and distinctive: 1) for different d, the ECC does not always change monotonically with $N_{\rm p}$; 2) the ECC of $d=0.1$ is higher than that of $d=0.5$ when $N_{\rm p}<150$, and vice versa when $N_{\rm p}>150$. In the NDET policy, there are two possible cases: one is that the two RF-powered nodes have the same RF power source, with the probability of 0.96 and 0.81 for $d=0.1$ and $d=0.5$, respectively; and the other is that the two

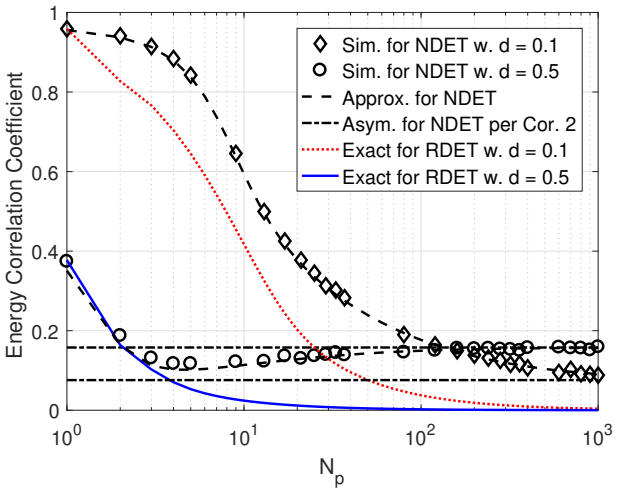

Fig. 3. The ECCs versus the antenna array size for the RDET and NDET.

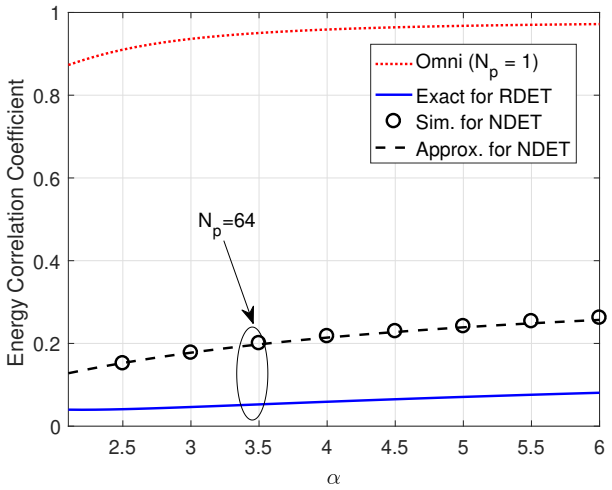

Fig. 4. The ECCs versus the path loss exponent for the RDET and NDET with $d = 0.1$.

RF-powered nodes have different nearest RF power sources. Thus, the reason behind the above observations is that the energy correlation is dominated by the former or the latter case, which depends on d and $N_{\rm p}$.

Fig. 4 shows how the path loss exponent α affects the ECC under different energy transfer policies for $d = 0.1$. It can be seen that for all three policies, i.e., the omni ($N_{\rm p} = 1$), RDET and NDET policies, the ECC grows slightly with the increase of α but with significant vertical gaps. This indicates that energy beamforming is a more crucial factor than the path loss in affecting the energy correlation in wirelessly powered networks, and a larger path loss exponent makes the nearby RF-power sources contribute a larger fraction of the total measured energy, which leads to a stronger energy correlation.

IV. Analysis of the Information Transmission Performance

In this section, we provide analytical results for the directed WET-enabled information transmission performance, incorporating the energy correlation induced by the RDET and NDET policies into the spatial configuration of the active transmitters (i.e., the energized RF-powered nodes). Since the probability generating functional (PGFL) of the EPP is unknown, it seems impossible to obtain an exact result on the success probability. Instead, due to the positive energy correlation, we resort to using the Matérn cluster process (MCP)[5] to approximate the EPP with the same first- and second-order statistics and obtaining an accurate approximation to the success probability. To that end, we first give the density of the EPP for the two directional energy transfer policies and then introduce the *energy correlation distance*, originated from the ECC, to determine the parameters of the MCP.

[5]Note that other cluster processes, such as the Thomas cluster process, may be equally suitable to approximate the EPP. However, the MCP is preferable due to its simplicity.

A. The Density of the EPP

For the RDET policy, the energies harvested at different RF-powered devices are identically distributed but not independent. Thus, denoting by $\lambda_{\rm e}$ the density of the EPP, we have $\lambda_{\rm e} = P_{\rm e}\lambda_{\rm d}$, where $P_{\rm e} \triangleq \mathbb{P}(\mathcal{E}_{\rm R}(o) > E_{\rm th})$ is the probability of harvesting enough energy at the device at the origin. The following theorem gives the density of the EPP under the RDET policy.

Theorem 3. *Let*

$$\mathcal{L}_{\rm R}(s) \triangleq \prod_{k\in\{\rm s,m\}} \exp\left(-\pi\lambda_{\rm p} q_k \int_0^\infty 1 - \frac{1}{\left(1+\frac{sG_k}{M(r^{\alpha/2}+\epsilon)}\right)^M} {\rm d}r \right). \tag{37}$$

The density of the EPP under the RDET policy is $\lambda_{\rm e} = P_{\rm e}\lambda_{\rm d}$, *where*

$$P_{\rm e} = 1 - \frac{1}{2\pi j}\int_{\gamma-j\infty}^{\gamma+j\infty} \frac{\exp(sE_{\rm th})}{s}\mathcal{L}_{\rm R}(s){\rm d}s, \tag{38}$$

where $j = \sqrt{-1}$ *and* $\gamma > 0$.

Proof: See Appendix D.

For the NDET policy, there are two types of RF-powered devices: those chosen to be directionally powered by their nearest RF power sources and those not chosen, which essentially harvest energy from the RF power sources with the RDET policy. The density of the EPP in the NDET policy depends on the energy harvesting success probabilities for both types of devices, which involve an approximation to the probability density function (PDF) of the area of the typical Voronoi cell. On this basis, we give an approximation to the density of the EPP under the NDET policy in the following theorem.

Theorem 4. *Let* $\varrho \triangleq 1-(1+\lambda_{\rm d}/(3.5\lambda_{\rm p}))^{-3.5}$,

$$\mathcal{L}_{\rm N1}(s) \triangleq \int_0^\infty \frac{\pi\lambda_{\rm p} e^{-\lambda_{\rm p}\pi r}}{\left(1+\frac{sG_{\rm m}}{M(r^{\alpha/2}+\epsilon)}\right)^M} \times \prod_{k\in\{s,m\}} \exp\Big(-\pi\lambda_{\rm p}\varrho q_k \int_r^\infty 1 - \frac{1}{\left(1+\frac{sG_k}{M(t^{\alpha/2}+\epsilon)}\right)^M}{\rm d}t\Big){\rm d}r,$$

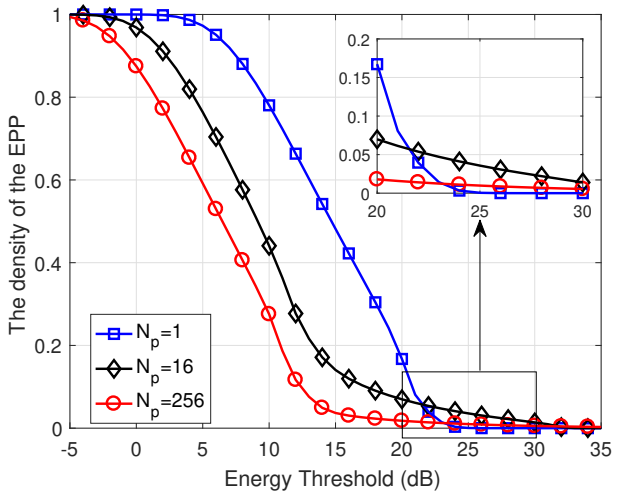

Fig. 5. The density versus the energy threshold for the RDET policy.

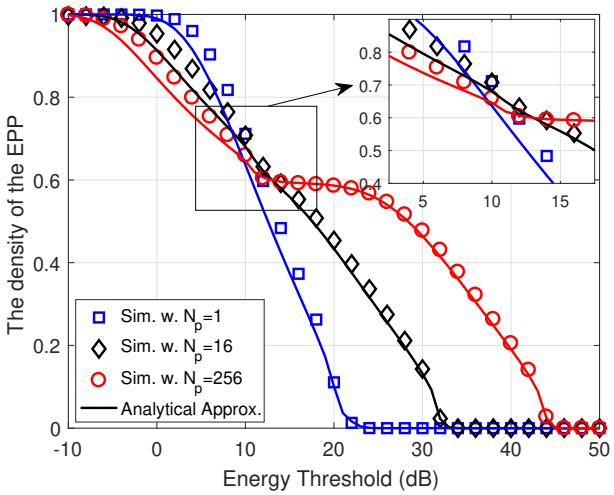

Fig. 6. The density versus the energy threshold for the NDET policy.

$$\mathcal{L}_{\mathrm{N2}}(s) \triangleq \prod_{k\in\{s,m\}} \exp\Big(-\pi\lambda_{\mathrm{p}}\varrho q_k \int_0^{\infty} 1-\frac{1}{\big(1+\frac{sG_k}{M(r^{\alpha/2}+\epsilon)}\big)^M}\mathrm{d}r\Big).$$

The density of the EPP under the NDET policy is approximated as $\lambda_{\mathrm{e}} \approx \lambda_{\mathrm{p}}\varrho P_{\mathrm{e}1} + (\lambda_{\mathrm{d}} - \lambda_{\mathrm{p}}\varrho)P_{\mathrm{e}2}$*, where*

$$P_{\mathrm{e}i} = 1 - \frac{1}{2\pi j}\int_{\gamma-j\infty}^{\gamma+j\infty} \frac{\exp(sE_{\mathrm{th}})}{s}\mathcal{L}_{\mathrm{N}i}(s)\mathrm{d}s, \quad i=1,2. \tag{39}$$

Proof: See Appendix E.

When $M \to \infty$, i.e., without fading in the energy transfer links, the Laplace transform of the measured energy can be further simplified as follows.

Corollary 4. *Letting* $M \to \infty$*, we have*

$$\mathcal{L}_{\mathrm{R}}(s) = \prod_{k\in\{\mathrm{s,m}\}} \exp\Big(-\pi\lambda_{\mathrm{p}} q_k \int_0^{\infty} 1-e^{-sG_k/(r^{\alpha/2}+\epsilon)}\mathrm{d}r\Big), \tag{40}$$

$$\mathcal{L}_{\mathrm{N1}}(s) = \int_0^{\infty} \pi\lambda_{\mathrm{p}} e^{-\lambda_{\mathrm{p}}\pi r - sG_{\mathrm{m}}/(r^{\alpha/2}+\epsilon)} \times \prod_{k\in\{\mathrm{s,m}\}} \exp\Big(-\pi\lambda_{\mathrm{p}}\varrho q_k \int_r^{\infty} 1-e^{-sG_k/(t^{\alpha/2}+\epsilon)}\mathrm{d}t\Big)\mathrm{d}r, \tag{41}$$

$$\mathcal{L}_{\mathrm{N2}}(s) = \prod_{k\in\{\mathrm{s,m}\}} \exp\Big(-\pi\lambda_{\mathrm{p}}\varrho q_k \int_0^{\infty} 1-e^{-sG_k/(r^{\alpha/2}+\epsilon)}\mathrm{d}r\Big). \tag{42}$$

Proof: The results are obtained by applying $\lim_{M\to\infty}(1+\frac{x}{M})^M = e^x$ to Thms. 3 and 4. ■

Remark 4. *Although both the RDET and NDET policies reduce to the omni-directional energy transfer case when* $N_{\mathrm{p}} = 1$*, the EPP densities for the two policies are different. In the RDET policy, all RF power sources are active, while in the NDET policy, an RF power source is active only if there is at least one RF-powered node in its Voronoi cell. As a result, if* $\lambda_{\mathrm{d}} \gg \lambda_{\mathrm{p}}$ *such that there exists at least one RF-powered node in almost all Voronoi cells, the EPP density is identical under the two policies; otherwise, the density of the EPP in the NDET policy is smaller than in the RDET policy.*

Fig. 5 plots the density of the EPP as a function of the energy threshold for the RDET policy with different antenna array sizes N_{p}. We observe that the density of the EPP decreases with increasing N_{p} for energy thresholds $E_{\mathrm{th}} < 20$ dB and the trend changes for $E_{\mathrm{th}} > 20$ dB where the case of $N_{\mathrm{p}} = 16$ surprisingly yields the highest EPP density for $E_{\mathrm{th}} > 23$ dB. The EPP density is an important indicator that represents the number of concurrently energized RF-powered nodes, which directly reflects the energy transfer performance. There are two competing aspects worth mentioning: 1) the omni-directional energy transfer policy provides smaller antenna gains than the RDET policy using beamforming technique; 2) more devices can be powered by the RF power sources thanks to the isotropic feature. Therefore, when the energy threshold is relatively low, the RF-powered nodes under the omni-directional energy transfer policy are easy to be energized, leading to a high EPP density. In constrast, when the energy threshold is relatively high, the RF-powered nodes harvest enough energy only through the energy beamforming technique. The reason why the EPP density for $N_{\mathrm{p}} = 256$ is smaller than for $N_{\mathrm{p}} = 16$ is that the randomly directed policy renders the main lobe of a narrower beam less likely to point in the right direction for the RF-powered nodes, which, in turn, stymies energization.

Fig. 6 plots the density of the EPP as a function of the energy threshold for the NDET policy with different antenna array sizes N_{p}. It can be seen that the approximate results match the simulations well, which shows the accuracy of the proposed approximation in Thm. 4, especially for high energy thresholds, i.e., $E_{\mathrm{th}} > 10$ dB. Besides, we observe that the EPP density increases with the decrease of N_{p} for about $E_{\mathrm{th}} < 10$ dB and vice versa when $E_{\mathrm{th}} > 10$ dB. For the former, the wider beam of a smaller antenna array supplies power to more RF-powered nodes which are easy to be energized for the low energy threshold, while for the latter, as the energy threshold increases, the demand for energy is getting higher, and the

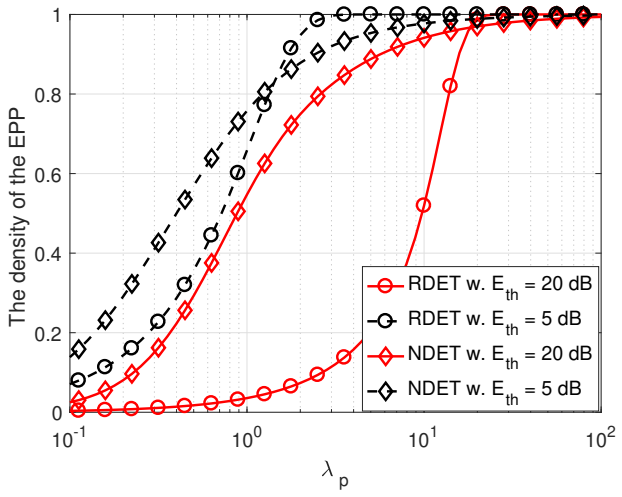

Fig. 7. The EPP density versus the density of RF power sources for both policies with $N_{\mathrm{p}} = 64$.

energy beamforming is becoming more important. There is an interesting observation in the case of $N_{\mathrm{p}} = 256$ that as E_{th} increases, the EPP density first decreases, then keeps almost unchanged for $10\,\mathrm{dB} < E_{\mathrm{th}} < 15\,\mathrm{dB}$ and continues to decrease to zero after that. In the early stage of increasing E_{th}, the aggregate signal strength from the side lobes also plays a part in energizing the RF-powered nodes, and when it comes to the range of $[10,\ 15]$ dB, the RF-powered nodes covered by the main lobes of the power sources are almost surely energized due to the high antenna gain of $G_{\mathrm{m}} = 256$. As E_{th} continues to increase, only the RF-powered nodes covered by the main lobes and close to the power sources can be energized, reducing the EPP density.

Fig. 7 compares the two directional energy transfer policies in terms of the EPP density. For different energy thresholds, the RDET policy energizes more RF-powered nodes than the NDET policy for large densities of RF power sources, for instance $\lambda_{\mathrm{p}} > 1.2$ for $E_{\mathrm{th}} = 5$ dB and $\lambda_{\mathrm{p}} > 11$ for $E_{\mathrm{th}} = 20$ dB. This observation comes from the difference in the objectives of the two policies: the RDET policy is to supply power without the location information of RF-powered node. Oppositely, the NDET policy just focuses on the precision of power supply to certain nodes. Thus, for a sparse deployment of RF power sources, the fraction of energized nodes under the RDET policy is lower than that under the NDET policy due to the high possibility of misalignment beam direction in the RDET case, while for a dense deployment of RF power sources, a part of RF power sources in the NDET case keep silent because of a lack of RF-powered nodes in their Voronoi cell, which does not occur in the RDET case. Conversely, a dense deployment helps compensate for the energy transfer loss caused by the randomness of the beam direction.

B. Success Probability

The information transmission success probability is defined as the complementary cumulative distribution function (CCDF) of the SIR, i.e., $P(\theta) \triangleq \mathbb{P}(\mathrm{SIR} > \theta)$, where θ is the SIR threshold. Letting $I^{!}_{\mathrm{EPP}} = \sum_{x \in \Phi^{!o}_{\mathrm{e}}} \ell_{\mathrm{I}}(x - z_{\mathrm{I}}) h_{x z_{\mathrm{I}}}$, the success probability can be derived through the Laplace transform $\mathcal{L}_{I^{!}_{\mathrm{EPP}}}(s) = \mathbb{E}(\exp(-sI^{!}_{\mathrm{EPP}}))$ of the interference via $P(\theta) = \mathcal{L}_{I^{!}_{\mathrm{EPP}}}(\theta d_{\mathrm{I}}^{\alpha})$. Due to the lack of a closed-form expression for the PGFL of the EPP, an exact characterization of $\mathcal{L}_{I^{!}_{\mathrm{EPP}}}(s)$ seems infeasible. Alternatively, we can find a point process with a similar spatial structure and a known conditional PGFL to approximate the EPP and characterize the success probability.

Motivated by the fact that an RF-powered device closer to RF-power sources is more likely to be energized and the measured energy at nearby devices is positively correlated, points in the EPP are distributed around the RF power sources and exhibit clustering behavior. Therefore, intuitively, the EPP can be well approximated by an MCP Φ_{M}, where the RF power sources are the parent point process, following a PPP with density λ_{p} and the points in each cluster are RF-powered nodes, placed uniformly at random in a disk of radius D around their parent points with the number of points in each cluster following a Poisson distribution with mean $\bar{c}$.

We determine the parameters D and $\bar{c}$ of the approximate MCP by matching first- and second-order statistics. To be specific, we first match the density $\lambda_{\mathrm{e}} = \lambda_{\mathrm{p}}\bar{c}$. Then, motivated by the feature that the pair correlation function of the MCP is 1 (indicating no correlation) when the distance is larger than $2D$, we establish a relationship between the parameter D and the distance corresponding to the ECC smaller than a sufficiently small value. To this end, we introduce the notion of the *ε-energy correlation distance*, defined as follows.

Definition 1. *For any $0 < \varepsilon < 1$, the ε-energy correlation distance D_{ε} is*

$$D_{\varepsilon} \triangleq \inf\{d_{\mathrm{c}} > 0 \colon \forall d > d_{\mathrm{c}}, \chi(d) < \varepsilon\}. \tag{43}$$

Here we set $\varepsilon = 0.001$ and $D = D_{\varepsilon}/2$ by assuming that the energy correlation vanishes if the distance is larger than the energy correlation distance. To sum up, the parameters of the approximated MCP follow: the density of the parent point process is λ_{p}, $\bar{c} = \lambda_{\mathrm{e}}/\lambda_{\mathrm{p}}$, and $D = D_{\varepsilon}/2$, where λ_{e} is obtained by Thms. 3 and 4.

Then, the Laplace transform of the interference in the EPP-based network can be approximated by that in the matched MCP-based network, i.e., $\mathcal{L}_{I^{!}_{\mathrm{EPP}}}(s) \approx \mathcal{L}_{I^{!}_{\mathrm{MCP}}}(s)$. According to [24, Eq. (34)], the Laplace transform of the interference is

$$\mathcal{L}_{I^{!}_{\mathrm{MCP}}}(s) = \exp\Big(-\lambda \int_{\mathbb{R}^2} 1 - e^{-\bar{c}\nu(s,y,z)} \mathrm{d}y\Big) \times \int_{b(o,D)} \frac{e^{-\bar{c}\nu(s,y,z)}}{\pi D^2} \mathrm{d}y, \tag{44}$$

where $\nu(s,y,z) = \frac{1}{\pi D^2} \int_{b(o,D)} \frac{1}{1+(s\ell_{\mathrm{I}}(x-y-z))^{-1}} \mathrm{d}x$. Thus, the success probability can be approximated as $P(\theta) \approx \mathcal{L}_{I^{!}_{\mathrm{MCP}}}(\theta d_{\mathrm{I}}^{\alpha})$, and we further obtain the area spectral efficiency (ASE) as

$$S(\theta) = \lambda_{\mathrm{e}} P(\theta) \log_2(1+\theta). \tag{45}$$

Since the density of the EPP λ_{e} decreases with the energy threshold while the information transmission success probability $P(\theta)$ increases with the decrease of λ_{e}, the ASE captures

TABLE II. The ε-energy correlation distance of different cases

RDET		NDET	
Case	$D_{0.001}$	Case	$D_{0.001}$
Omnidirectional, $\lambda_{\mathrm{p}}=1$	2.58	Omnidirectional, $\lambda_{\mathrm{p}}=1$	2.58
$N_{\mathrm{p}}=64, \lambda_{\mathrm{p}}=1$	0.78	$N_{\mathrm{p}}=64, \lambda_{\mathrm{p}}=1$	1.66
$N_{\mathrm{p}}=256, \lambda_{\mathrm{p}}=1$	0.48	$N_{\mathrm{p}}=256, \lambda_{\mathrm{p}}=1$	1.66
$N_{\mathrm{p}}=64, \lambda_{\mathrm{p}}=0.1$	0.78	$N_{\mathrm{p}}=64, \lambda_{\mathrm{p}}=0.1$	3.88

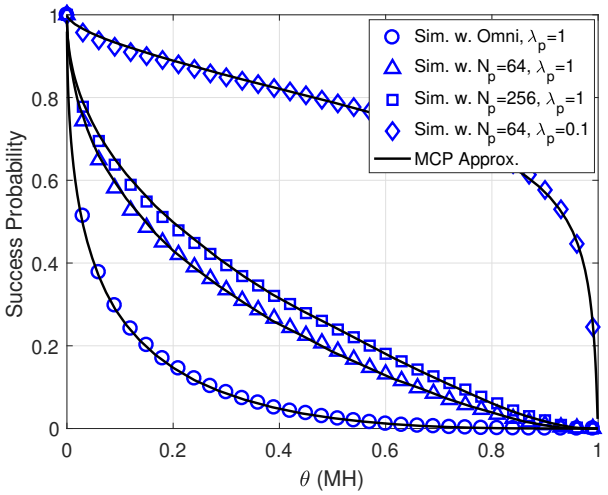

Fig. 8. The success probability in MH for the RDET policy with $E_{\mathrm{th}} = 10$ dB.

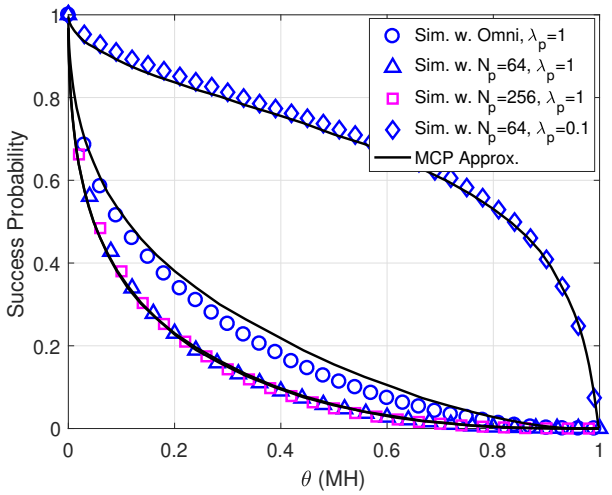

Fig. 9. The success probability in MH for the NDET policy with $E_{\mathrm{th}} = 15$ dB.

the trade-off between the performance in the energy transfer and information transmission phases.

Table II gives the ε-energy correlation distance for different cases with $\varepsilon = 0.001$, which is used to determine the parameters in the MCP-based approximation in calculating the success probability shown in Fig. 8 and Fig. 9. From Thm. 1, the ECC of the RDET policy is independent of the density of RF power sources, and thus it holds for the corresponding ε-energy correlation distance. Since the SIR threshold in linear unit is $\theta \in \mathbb{R}^+$ (or $\theta \in \mathbb{R}$ in dB form), a plot showing the success probability as a function of θ or θ in dB cannot reveal the complete information. Hence, we plot it in *Möbius homeomorphic* units, abbreviated to MH, via the transformation $\theta\,(\mathrm{MH}) = \theta/(1+\theta)$, resulting in $\theta\,(\mathrm{MH}) \in [0,1]$ [25] in Fig. 8 and Fig. 9. Interpreted differently, the figures show the CCDF of the signal fraction in a linear scale. The two figures compare the EPP-based simulations with the MCP-based analytical results under the RDET and NDET policies, respectively, for different λ_{p} and N_{p}. It is observed that for different parameter sets, the MCP-based approximations match the simulated results quite well. This validates the accuracy of the proposed ECC-based approximation where the parameters of the MCP are determined with the aid of the ε-energy correlation distance. Furthermore, for a given RF power source density, the omni-directional case in the RDET policy yields the worst performance since it energizes the most concurrent communication links. However, for the NDET policy, the antenna array size does not have a significant effect on the success probability, e.g., the cases of $N_{\mathrm{p}} = 64, 256$ have almost the same performance which is slightly worse than for $N_{\mathrm{p}} = 1$. These observations imply that the success probability in the communication phase is closely related to the EPP density, which, in turn, is closely related to the performance in the energy transfer phase.

Fig. 10 and Fig. 11 compare the two energy transfer policies in terms of the success probability and the ASE, respectively. It is observed that for both performance indicators, the MCP-based approximations match the simulation results well for a large range of the energy threshold, which again demonstrates the accuracy and effectiveness of the proposed approximation method. Furthermore, for a given energy threshold, the RDET policy always provides a better success probability than the NDET policy due to the smaller density of the EPP in the former case for $N_{\mathrm{p}} = 64$ and $\lambda_{\mathrm{p}} = 0.1$. The success probability in the communication phase is closely related to the EPP density since fewer energized RF-powered nodes cause less interference which leads to higher success probability. For the ASE performance, different SIR thresholds lead to entirely different trends of the ASE curve. For $\theta = -10$ dB, the ASEs for both policies decrease with the energy threshold E_{th} and the performance of the NDET is always better than that of the RDET, but there is a practical limit such that E_{th} cannot go to zero, i.e., there should be a lower bound for E_{th} in practice. For $\theta = 15$ dB, for the given parameter setting, there is an optimal energy threshold[6] that leads to the maximum ASE, and the optimal one in the RDET policy is smaller than that in the NDET policy. The reason behind these observations lies in the

[6]We are not assuming that there is a fixed type of hardware being used here. Hence if an optimum energy threshold is found, then the hardware could be engineered accordingly.

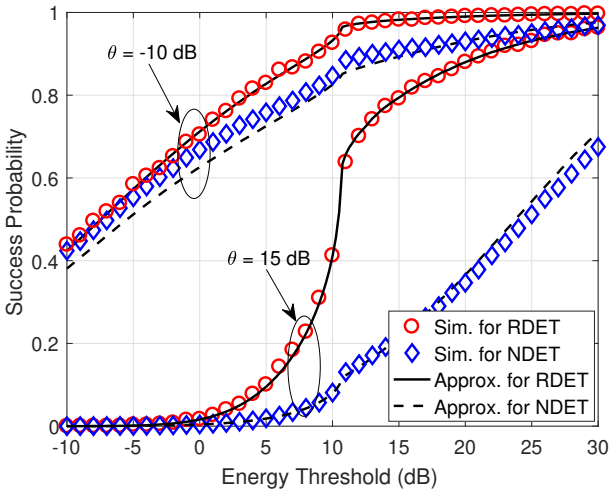

Fig. 10. The success probability versus the energy threshold for different policies with $N_{\mathrm{p}} = 64$.

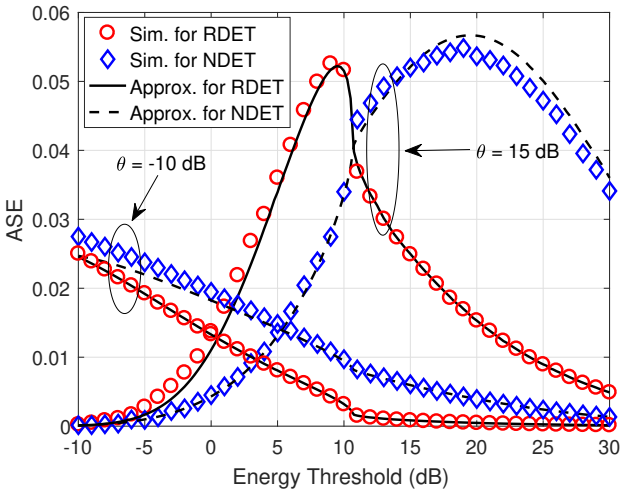

Fig. 11. The ASE versus the energy threshold for different policies with $N_{\mathrm{p}} = 64$.

trade-off between the performance in the energy transfer and information transmission phases. In the energy transfer phase, it is sensible to try to energize as many RF-powered nodes as possible, i.e., to try to increase the EPP density, while in the communication phase, a larger density of the EPP will in turn cause a lower success probability. The ASE reflects this trade-off.

V. Conclusions

In this paper, we introduced the ECC, which is the correlation coefficient of the harvested energies at two locations, to investigate the energy correlation in a wirelessly powered network with energy beamforming. We fully characterized the ECC for a Poisson field of RF power sources that transfer the energy directionally through two energy beamforming policies, i.e., the RDET and NDET policies. The key insight is that the energy harvested from directed RF beams are spatially correlated and the energized RF-powered nodes exhibit attraction, which should be taken into account when analyzing the WET-enabled communication performance. Besides, we found that the introduction of the energy beamforming technique weakens the energy correlation relative to the omni-directional case, and when $N_{\mathrm{p}} \to \infty$, the energy correlation vanishes for the RDET but approaches a non-zero constant for the NDET. The NDET policy requires prior information (the positions of the RF-powered nodes) in order to precisely point the beam to the target powered node and the RDET policy does not but instead it may waste much energy due to the misaligned beam direction.

To show the key role of the ECC in the wirelessly powered communication phase, we proposed the application of the ECC in characterizing the second-order statistic of the EPP and provided an MCP approximation to the EPP where the parameters of the MCP can be directly obtained through the energy correlation distance. The results demonstrate that the proposed MCP-based approximations match the actual success probability and ASE extremely accurately. Although the ECC is an average quantity and does not provide the complete distribution of the joint energy harvesting performance at two locations, it neatly circumvents both the complex analysis of the pcf and the classic point process fitting. Hence it enables the handling of the spatial correlation issue in more general and complicated networks. Moreover, since the energy correlation equals the interference correlation under the same path loss and fading models, the results of the ECC also apply to the interference correlation with directional beamforming.

Appendix A
Proof of Lemma 1

Proof: As shown in the left figure of Fig. 12, ν denotes the angle between the directions from x to o and $z = (d, 0)$, and according to the cosine law, we have

$$\nu = \arccos\left(\frac{r - d\cos\theta}{\sqrt{r^2 + d^2 - 2rd\cos\theta}}\right). \tag{46}$$

The value of $\widetilde{G}(x, z)$ depends on the relative angle relationship between ν and the beam direction. We first consider the case of $\nu \geq w$ and $\widetilde{G}(x, z)$ can be either G_{s}^2 or $G_{\mathrm{m}}G_{\mathrm{s}}$. Since the beam direction is uniformly distributed in $[0, 2\pi]$, the probability of merely one direction (either $x \to z$ or $x \to o$) lying in the beam is $\frac{2w}{2\pi}$. Thus, we have

$$\widetilde{G}(x, z) = \begin{cases} G_{\mathrm{m}}G_{\mathrm{s}} & \text{w.p. } \frac{w}{\pi} \\ G_{\mathrm{s}}^2 & \text{w.p. } 1 - \frac{w}{\pi}. \end{cases} \tag{47}$$

For the case of $\nu < w$, the probability of the two directions (both $x \to z$ and $x \to o$) lying in the beam is $\frac{w-\nu}{2\pi}$, and then the probability of merely one direction (either $x \to z$ or $x \to o$) lying in the beam is $\frac{2\nu}{2\pi}$. Hence, we have

$$\widetilde{G}(x, z) = \begin{cases} G_{\mathrm{m}}^2 & \text{w.p. } \frac{w-\nu}{2\pi} \\ G_{\mathrm{m}}G_{\mathrm{s}} & \text{w.p. } \frac{\nu}{\pi} \\ G_{\mathrm{s}}^2 & \text{w.p. } 1 - \frac{w+\nu}{2\pi}. \end{cases} \tag{48}$$

Combining the above two cases, the final result is obtained. ■

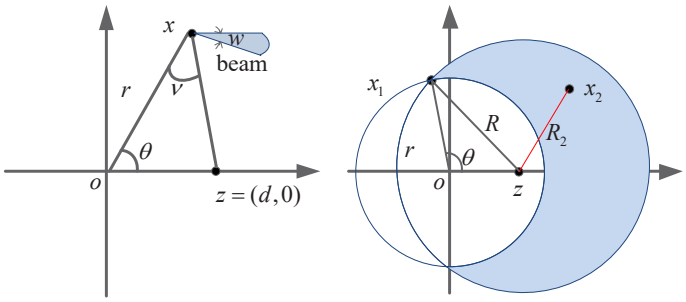

Fig. 12. Illustrations for the proofs of Lemma 1 (left) and Lemma 2 (right).

Appendix B
Proof of Lemma 2

Proof: As shown in the right figure of Fig. 12, x_1 is the nearest RF power source to the origin o and R denotes the distance from x_1 to z. We first derive the probability of o and z having the same nearest RF power source x_1, which is equivalent to the case that no RF power source is in the shadow region. Then the corresponding probability of this event is given by

$$\varpi(r,\theta) = e^{-\lambda_{\rm p}(\pi R^2 - A(R,r,d))}, \tag{49}$$

where $\pi R^2 - A(R,r,d)$ is the area of the shadow region. The unconditional probability is obtained by using the contact distance distribution of the PPP $f_{\|x_1\|}(r) = 2\pi\lambda_{\rm p} r e^{-\pi\lambda_{\rm p} r^2}$ [26] and the angle θ of x_1 randomly uniformly distributed in $[0, 2\pi)$, and we have

$$\begin{aligned} p_{\rm same} &= \int_0^{2\pi}\int_0^{\infty} \frac{1}{2\pi} f_{\|x_1\|}(r)\varpi(r,\theta)\mathrm{d}r\mathrm{d}\theta \\ &\overset{(a)}{=} \int_0^{\pi}\int_0^{\infty} 2\lambda_{\rm p} r e^{-\pi\lambda_{\rm p} r^2}\varpi(r,\theta)\mathrm{d}r\mathrm{d}\theta, \end{aligned} \tag{50}$$

where step (a) follows from the symmetry of $\varpi(r,\theta)$ over $\theta \in [0,\pi]$ and $[\pi, 2\pi]$.

Secondly, conditioned on z having a different nearest RF power source x_2, the cumulative distribution function of the distance from x_2 to z, denoted by R_2, is given by

$$\begin{aligned} F_{R_2}(r_2) &= \mathbb{P}(R_2 < r_2 \mid x_2 \neq x_1) \\ &= \frac{\mathbb{P}(\mathcal{X})}{1 - e^{-\lambda_{\rm p}(\pi R^2 - A(R,r,d))}}, \end{aligned} \tag{51}$$

where $\mathcal{X}$ denotes the event that there is no RF power source in the region $b(z,r_2) \setminus b(z,r_2) \cap b(o,r)$, whose probability is

$$\mathbb{P}(\mathcal{X}) = 1 - e^{-\lambda_{\rm p}(\pi r_2^2 - A(r_2,r,d))}. \tag{52}$$

According to the geometrical relationship, we further obtain $R_2 \in [\max(0, r-d), R]$. ∎

Appendix C
Proof of Theorem 2

Proof: Using the contact distance distribution of the PPP $f_{\|x_1\|}(r) = 2\pi\lambda_{\rm p} r e^{-\pi\lambda_{\rm p} r^2}$ [26], it is easy to derive the first- and second-order moments of the approximate measured energy at the origin $\mathcal{E}_{\rm N}(o)$. For $\mathcal{E}_{\rm N}(z)$, its expectation is approximated as

$$\begin{aligned} \mathbb{E}\mathcal{E}_{\rm N}(z) &\approx \mathbb{E}[G(\varphi_{x_1}(z))h_{x_1 z}\ell(x_1 - z)\mathbf{1}_{x_2 = x_1} \\ &\quad + G_{\rm m} h_{x_2 z}\ell(x_2 - z)\mathbf{1}_{x_2 \neq x_1}] \\ &= \int_0^{2\pi}\int_0^{\infty} \frac{f_{\|x_1\|}(r)}{2\pi}\Big(\frac{\varpi(r,\theta)\hat{G}(r,\theta)}{\epsilon + \|x_1 - z\|^{\alpha}} \\ &\quad + \mathbb{E}_{R_2}\frac{(1-\varpi(r,\theta))G_{\rm m}}{\epsilon + R_2^{\alpha}}\Big)\mathrm{d}r\mathrm{d}\theta \\ &= 2\lambda_{\rm p}\int_0^{\pi}\int_0^{\infty} r e^{-\pi\lambda_{\rm p} r^2}\Big(\frac{\varpi(r,\theta)\hat{G}(r,\theta)}{\epsilon + R^{\alpha}} \\ &\quad + \int_{\psi(r)}^{R}\frac{G_{\rm m}(1-\varpi(r,\theta))\mathrm{d}F_{R_2}(r_2)}{\epsilon + r_2^{\alpha}}\Big)\mathrm{d}r\mathrm{d}\theta, \end{aligned} \tag{53}$$

where $\varpi(r,\theta)$ is the conditional probability of the two locations z and o having the same nearest RF power source x_1, $\hat{G}(r,\theta)$ is the array gain from x_1 to z when the beam of x_1 is pointed to o, and $R_2 = \|x_2 - z\|$. As shown in the left figure of Fig. 12, $\hat{G}(r,\theta)$ depends on the angle ν between the directions from x to o and z, and $\hat{G}(r,\theta) = G_{\rm m}$ if ν is in the range of the beam from x_1 to o, otherwise $\hat{G}(r,\theta) = G_{\rm s}$. Similarly, we obtain the second moment of $\mathcal{E}_{\rm N}(z)$. For the mean of $\mathcal{E}_{\rm N}(o)\mathcal{E}_{\rm N}(z)$, we have

$$\begin{aligned} &\mathbb{E}[\mathcal{E}_{\rm N}(o)\mathcal{E}_{\rm N}(z)] \\ &= \mathbb{E}[G_{\rm m} h_{x_1 o}\ell(x_1)G(\varphi_{x_1}(z))h_{x_1 z}\ell(x_1 - z)\mathbf{1}_{x_2 = x_1} \\ &\quad + G_{\rm m}^2 h_{x_1 o}\ell(x_1)h_{x_2 z}\ell(x_2 - z)\mathbf{1}_{x_2 \neq x_1}] \\ &= 2\lambda_{\rm p} G_{\rm m}\int_0^{\pi}\int_0^{\infty} r e^{-\pi\lambda_{\rm p} r^2}\Big(\frac{\varpi(r,\theta)\hat{G}(r,\theta)}{(\epsilon + r^{\alpha})(\epsilon + R^{\alpha})} \\ &\quad + \mathbb{E}_{R_2}\frac{(1-\varpi(r,\theta))G_{\rm m}}{(\epsilon + r^{\alpha})(\epsilon + R_2^{\alpha})}\Big)\mathrm{d}r\mathrm{d}\theta \\ &= 2\lambda_{\rm p} G_{\rm m}\int_0^{\pi}\int_0^{\infty} r e^{-\pi\lambda_{\rm p} r^2}\Big(\frac{\varpi(r,\theta)\hat{G}(r,\theta)}{\epsilon + R^{\alpha}} \\ &\quad + \int_{\psi(r)}^{R}\frac{G_{\rm m}(1-\varpi(r,\theta))\mathrm{d}F_{R_2}(r_2)}{\epsilon + r_2^{\alpha}}\Big)\mathrm{d}r\mathrm{d}\theta. \end{aligned} \tag{54}$$

Substituting the above results into (3), the final result is obtained. ∎

Appendix D
Proof of Theorem 3

Proof: Under the RDET policy, the measured energy of the typical device at the origin is $\varepsilon(x, \Phi_{\rm p}) = \mathcal{E}_{\rm R}(o)$, and the Laplace transform of $\mathcal{E}_{\rm R}(o)$ is given by

$$\begin{aligned} \mathcal{L}_{\rm R}(s) &= \mathbb{E}\Big[\prod_{x\in\Phi_{\rm p}}\frac{1}{(1 + \frac{sG(\varphi_x(o))\ell(x)}{M})^M}\Big] \\ &= \mathbb{E}\Big[\prod_{x\in\Phi_{\rm p}}\Big(\frac{q_{\rm m}}{(1 + \frac{sG_{\rm m}\ell(x)}{M})^M} + \frac{q_{\rm s}}{(1 + \frac{sG_{\rm s}\ell(x)}{M})^M}\Big)\Big] \\ &= \prod_{k\in\{\rm s,m\}}\exp\Big(-\pi\lambda_{\rm p} q_k\int_0^{\infty} 1 - \frac{1}{\big(1 + \frac{sG_k}{M(r^{\alpha/2} + \epsilon)}\big)^M}\mathrm{d}r\Big). \end{aligned} \tag{55}$$

Through the inverse Laplace transform, we have

$$\mathbb{P}(\mathcal{E}_{\mathrm{R}}(o) > E_{\mathrm{th}}) = 1 - \frac{1}{2\pi j}\int_{\gamma-j\infty}^{\gamma+j\infty} \frac{\exp(sE_{\mathrm{th}})}{s}\mathcal{L}_{\mathrm{R}}(s)\mathrm{d}s, \tag{56}$$

where $j = \sqrt{-1}$ and γ is a real number so that the path of integration is in the region of convergence (ROC) of $\mathcal{L}_{\mathrm{R}}(s)$. Since $\mathcal{E}_{\mathrm{R}}(o)$ is non-negative, the ROC is $\mathrm{Re}\{s\} > \mathrm{Re}\{P_0\}$, where P_0 is the singularity of $\mathcal{L}_{\mathrm{R}}(s), s \in \mathbb{C}$, with the maximum real part, and it contains the region of $\mathrm{Re}\{s\} > 0$, because there is no singularity when $\mathrm{Re}\{s\} > 0$. Thus, γ can be chosen as any positive number. ■

Appendix E
Proof of Theorem 4

Proof: Let $\Phi_{\mathrm{d1}}, \lambda_{\mathrm{d1}}, P_{\mathrm{e1}}$ be the devices which are chosen to be powered directionally by their nearest RF power sources, the corresponding density and the success probability of energy harvesting, $\Phi_{\mathrm{d2}}, \lambda_{\mathrm{d2}}, P_{\mathrm{e2}}$ be the remaining devices, the corresponding density and the success probability of energy harvesting, respectively, and we have $\Phi_{\mathrm{d}} = \Phi_{\mathrm{d1}} \cup \Phi_{\mathrm{d2}}$ and $\lambda_{\mathrm{d}} = \lambda_{\mathrm{d1}} + \lambda_{\mathrm{d2}}$. Thus, the density of the EPP is $\lambda_{\mathrm{e}} = P_{\mathrm{e1}}\lambda_{\mathrm{d1}} + P_{\mathrm{e2}}\lambda_{\mathrm{d2}}$.

For Φ_{d1}, its density is equal to that of the RF power sources which have devices to be powered in their Voronoi cells, i.e., $\lambda_{\mathrm{d1}} = \lambda_{\mathrm{p}}\varrho$, where ϱ is the probability that there is at least one device in a Voronoi cell. Using the total probability law, we have

$$\begin{aligned}\varrho &= \int_0^\infty (1 - e^{-\lambda_{\mathrm{d}}x}) f_S(x)\mathrm{d}x \\ &\approx 1 - (1 + \lambda_{\mathrm{d}}/(3.5\lambda_{\mathrm{p}}))^{-3.5},\end{aligned} \tag{57}$$

where $f_S(x)$ is the PDF of the area S of the typical Voronoi cell for a PPP, approximated by [27, 28],

$$f_S(x) \approx \frac{343}{15}\sqrt{\frac{3.5}{\pi}}(x\lambda_{\mathrm{p}})^{2.5}e^{-3.5x\lambda_{\mathrm{p}}}\lambda_{\mathrm{p}}. \tag{58}$$

For the devices in Φ_{d1}, the measured energy of the typical device at the origin is

$$\begin{aligned}\varepsilon(x, \Phi_{\mathrm{p}}) &= \mathcal{E}_{\mathrm{N1}}(o) \\ &= G_{\mathrm{m}}h_{x_1o}\ell(x_1) + \sum_{x\in\tilde{\Phi}_{\mathrm{p}}\setminus\{x_1\}} G(\varphi_x(o))h_{xo}\ell(x),\end{aligned} \tag{59}$$

where x_1 denotes the nearest RF power source in Φ_{p} and $\tilde{\Phi}_{\mathrm{p}}$ denotes all the active RF power sources in Φ_{p}. The Laplace transform of $\mathcal{E}_{\mathrm{N1}}(o)$ is given by

$$\begin{aligned}\mathcal{L}_{\mathrm{N1}}(s) =& \mathbb{E}\Big[\frac{1}{(1 + \frac{sG_{\mathrm{m}}\ell(x_1)}{M})^M} \\ &\times \prod_{x\in\tilde{\Phi}_{\mathrm{p}}\setminus\{x_1\}} \frac{1}{(1 + \frac{sG(\varphi_x(o))\ell(x)}{M})^M}\Big] \\ \overset{(a)}{\approx}& \int_0^\infty \frac{f_{\|x_1\|}(r)}{\big(1 + \frac{sG_{\mathrm{m}}}{M(r^\alpha+\epsilon)}\big)^M} \\ &\times \exp\Big(-\pi\lambda_{\mathrm{p}}\varrho\int_r^\infty \Big(1 - \sum_{k\in\{\mathrm{s,m}\}} \frac{q_k}{\big(1 + \frac{sG_k}{M(t^{\alpha/2}+\epsilon)}\big)^M}\Big)t\mathrm{d}t\Big)\mathrm{d}r \\ =& \int_0^\infty \frac{\pi\lambda_{\mathrm{p}}e^{-\lambda_{\mathrm{p}}\pi r}}{\big(1 + \frac{sG_{\mathrm{m}}}{M(r^{\alpha/2}+\epsilon)}\big)^M} \\ &\times \prod_{k\in\{\mathrm{s,m}\}} \exp\Big(-\pi\lambda_{\mathrm{p}}\varrho q_k\int_r^\infty 1 - \frac{1}{\big(1+\frac{sG_k}{M(t^{\alpha/2}+\epsilon)}\big)^M}\mathrm{d}t\Big)\mathrm{d}r,\end{aligned} \tag{60}$$

where step (a) follows from the contact distance distribution of the PPP $f_{\|x_1\|}(r) = 2\pi\lambda_{\mathrm{p}}re^{-\pi\lambda_{\mathrm{p}}r^2}$ [26] and $\tilde{\Phi}_{\mathrm{p}}$ is approximated as an independent thinning of Φ_{p} with probability ϱ. Through the inverse Laplace transform, we obtain the success probability P_{e1}.

The density of Φ_{d2} is $\lambda_{\mathrm{d2}} = \lambda_{\mathrm{d}} - \lambda_{\mathrm{p}}\varrho$, and the Laplace transform $\mathcal{L}_{\mathrm{N2}}(s)$ of the measured energy $\mathcal{E}_{\mathrm{N2}}(o)$ at the devices in Φ_{d2} can be derived similarly to that in the RDET case, i.e., modifying the density of RF power sources as $\lambda_{\mathrm{p}}\varrho$. Then the energy harvesting success probability P_{e2} follows from the inverse Laplace transform. ■

References

[1] N. Deng and M. Haenggi, "Energy correlation coefficient in wirelessly powered networks with energy beamforming," in *IEEE International Conference on Communications (ICC'21)*, Montreal, Canada, June 2021.

[2] S. Bi, C. K. Ho, and R. Zhang, "Wireless powered communication: opportunities and challenges," *IEEE Communications Magazine*, vol. 53, no. 4, pp. 117–125, Apr. 2015.

[3] X. Lu, P. Wang, D. Niyato, D. I. Kim, and Z. Han, "Wireless charging technologies: Fundamentals, standards, and network applications," *IEEE Communications Surveys & Tutorials*, vol. 18, no. 2, pp. 1413–1452, 2016.

[4] S. Khairy, M. Han, L. X. Cai, and Y. Cheng, "Sustainable wireless IoT networks with RF energy charging over Wi-Fi (CoWiFi)," *IEEE Internet of Things Journal*, vol. 6, no. 6, pp. 10 205–10 218, 2019.

[5] K. Huang and V. K. N. Lau, "Enabling wireless power transfer in cellular networks: Architecture, modeling and deployment," *IEEE Transactions on Wireless Communications*, vol. 13, no. 2, pp. 902–912, Feb. 2014.

[6] L. Shi, L. Zhao, K. Liang, and H. Chen, "Wireless energy transfer enabled D2D in underlaying cellular networks," *IEEE Transactions on Vehicular Technology*, vol. 67, no. 2, pp. 1845–1849, Feb 2018.

[7] X. Zhou, J. Guo, S. Durrani, and M. Di Renzo, "Power beacon-assisted millimeter wave ad hoc networks," *IEEE Transactions on Communications*, vol. 66, no. 2, pp. 830–844, Feb 2018.

[8] N. Deng and M. Haenggi, "The energy and rate meta distributions in wirelessly powered D2D networks," *IEEE Journal on Selected Areas in Communications*, vol. 37, no. 2, pp. 269–282, 2019.

[9] S. K. Nobar, J. M. Niya, and B. M. Tazehkand, "Performance analysis of cognitive wireless powered communication networks under unsaturated traffic condition," *IEEE Transactions on Green Communications and Networking*, vol. 4, no. 3, pp. 819–831, 2020.

[10] N. Deng and M. Haenggi, "The energized point process as a model for wirelessly powered communication networks," *IEEE Transactions on Green Communications and Networking*, vol. 4, no. 3, pp. 832–844, 2020.

[11] M. Haenggi, *Stochastic geometry for wireless networks*. Cambridge University Press, 2012.

[12] N. Deng and M. Haenggi, "A tractable model for wirelessly powered networks with energy correlation," *IEEE Transactions on Wireless Communications*, vol. 19, no. 9, pp. 5765–5778, 2020.

[13] Y. Alsaba, S. K. A. Rahim, and C. Y. Leow, "Beamforming in wireless energy harvesting communications systems: A survey," *IEEE Communications Surveys Tutorials*, vol. 20, no. 2, pp. 1329–1360, 2018.

[14] I. Krikidis, S. Timotheou, S. Nikolaou, G. Zheng, D. W. K. Ng, and R. Schober, "Simultaneous wireless information and power transfer in modern communication systems," *IEEE Communications Magazine*, vol. 52, no. 11, pp. 104–110, 2014.

[15] M. Di Renzo and W. Lu, "System-level analysis and optimization of cellular networks with simultaneous wireless information and power transfer: Stochastic geometry modeling," *IEEE Transactions on Vehicular Technology*, vol. 66, no. 3, pp. 2251–2275, March 2017.

[16] C. Liu and C. Hsu, "Fundamentals of simultaneous wireless information and power transmission in heterogeneous networks: A cell-load perspec-

tive," *IEEE Journal on Selected Areas in Communications*, vol. 37, no. 1, pp. 100–115, 2019.
[17] A. H. Sakr and E. Hossain, "Analysis of K-tier uplink cellular networks with ambient RF energy harvesting," *IEEE Journal on Selected Areas in Communications*, vol. 33, no. 10, pp. 2226–2238, 2015.
[18] M. A. Kishk and H. S. Dhillon, "Joint uplink and downlink coverage analysis of cellular-based RF-powered IoT network," *IEEE Transactions on Green Communications and Networking*, vol. 2, no. 2, pp. 446–459, 2018.
[19] S. Singh, M. N. Kulkarni, A. Ghosh, and J. G. Andrews, "Tractable model for rate in self-backhauled millimeter wave cellular networks," *IEEE Journal on Selected Areas in Communications*, vol. 33, no. 10, pp. 2196–2211, Oct. 2015.
[20] N. Deng, M. Haenggi, and Y. Sun, "Millimeter-wave device-to-device networks with heterogeneous antenna arrays," *IEEE Transactions on Communications*, vol. 66, no. 9, pp. 4271–4285, Sep. 2018.
[21] A. Jeffrey and D. Zwillinger, *Table of integrals, series, and products*. Academic Press, 2007.
[22] R. K. Ganti and M. Haenggi, "Spatial and temporal correlation of the interference in ALOHA ad hoc networks," *IEEE Communications Letters*, vol. 13, no. 9, pp. 631–633, 2009.
[23] Z. Gong and M. Haenggi, "Interference and outage in mobile random networks: Expectation, distribution, and correlation," *IEEE Transactions on Mobile Computing*, vol. 13, no. 2, pp. 337–349, 2014.
[24] R. Ganti and M. Haenggi, "Interference and outage in clustered wireless ad hoc networks," *IEEE Transactions on Information Theory*, vol. 55, no. 9, pp. 4067–4086, 2009.
[25] M. Haenggi, "SIR analysis via signal fractions," *IEEE Communications Letters*, vol. 24, no. 7, pp. 1358–1362, July 2020.
[26] M. Haenggi, "On distances in uniformly random networks," *IEEE Transactions on Information Theory*, vol. 51, no. 10, pp. 3584–3586, Oct. 2005.
[27] J. Ferenc and Z. Neda, "On the size distribution of Poisson Voronoi cells," *Physica A-Statistical Mechanics and Its Applications*, vol. 385, no. 2, pp. 518–526, 2007.
[28] N. Deng, W. Zhou, and M. Haenggi, "Heterogeneous cellular network models with dependence," *IEEE Journal on Selected Areas in Communications*, vol. 33, no. 10, pp. 2167–2181, 2015.

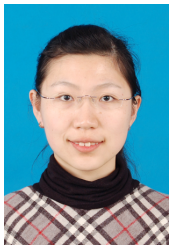

Na Deng (S'12-M'17) received the B.S. and Ph.D. degrees in information and communication engineering from the University of Science and Technology of China (USTC), Hefei, China, in 2010 and 2015, respectively. Currently she is an Associate Professor at Dalian University of Technology, Dalian, China. In 2013-2014, she was a Visiting Student in Prof. Martin Haenggi's group at the University of Notre Dame, Notre Dame, IN, USA, and in 2015-2016 she was a Senior Engineer at Huawei Technologies Co., Ltd., Shanghai, China. Her scientific interests include networking and wireless communications, intelligent communications, and space-air-ground integrated networks.

Martin Haenggi (S'95-M'99-SM'04-F'14) received the Dipl.-Ing. (M.Sc.) and Dr.sc.techn. (Ph.D.) degrees in electrical engineering from the Swiss Federal Institute of Technology in Zurich (ETH) in 1995 and 1999, respectively. Currently he is the Freimann Professor of Electrical Engineering and a Concurrent Professor of Applied and Computational Mathematics and Statistics at the University of Notre Dame, Indiana, USA. In 2007-2008, he was a Visiting Professor at the University of California at San Diego, and in 2014-2015 he was an Invited Professor at EPFL, Switzerland, and in 2021-2022 he is a Guest Professor at ETHZ. He is a co-author of the monographs "Interference in Large Wireless Network" (NOW Publishers, 2009) and "Stochastic Geometry Analysis of Cellular Networks" (Cambridge University Press, 2018) and the author of the textbook "Stochastic Geometry for Wireless Networks" (Cambridge, 2012) and the blog stogblog.net, and he published 18 single-author journal articles. His scientific interests lie in networking and wireless communications, with an emphasis on cellular, amorphous, ad hoc (including D2D and M2M), cognitive, vehicular, and wirelessly powered networks. He served as an Associate Editor for the Elsevier Journal of Ad Hoc Networks, the IEEE Transactions on Mobile Computing (TMC), the ACM Transactions on Sensor Networks, as a Guest Editor for the IEEE Journal on Selected Areas in Communications, the IEEE Transactions on Vehicular Technology, and the EURASIP Journal on Wireless Communications and Networking, as a Steering Committee member of the TMC, and as the Chair of the Executive Editorial Committee of the IEEE Transactions on Wireless Communications (TWC). From 2017 to 2018, he was the Editor-in-Chief of the TWC. Currently he is an editor for MDPI Information. For both his M.Sc. and Ph.D. theses, he was awarded the ETH medal. He also received a CAREER award from the U.S. National Science Foundation in 2005 and three paper awards from the IEEE Communications Society, the 2010 Best Tutorial Paper award, the 2017 Stephen O. Rice Prize paper award, and the 2017 Best Survey paper award, and he is a Clarivate Analytics Highly Cited Researcher.